7.1 Soil Formation

R Amundson, University of California, Berkeley, CA, USA

"Man has only a thin layer of soil between himself and starvation"
attributed to the Bard of Cincinnati

7.1.1 Introduction

Soil is the epidermis of a terrestrial planet, a veneer that lies at the interface between the lithosphere and the atmosphere. Due to heat, gas, and water/solute transport between soil and the atmosphere, soil properties are highly depth dependent, and the interpretation of soil measurements commonly requires a combination of tools from physics, hydrology, geochemistry, and other fields – with field skills derived from geomorphology and geology. Soil forms with or without biology, and while life certainly imparts unique characteristics to soils, its absence does not impinge on many other geochemical processes that continue to impact the soils. In that vein, the lifeless or nearly lifeless places on Earth are highly illuminating as analogs for soils reflecting the now dry and abiotic Mars. This chapter presents an abridged overview of the factors and processes that form the soil *derma* and is with a few exceptions a major revision of a chapter that appeared in the first edition of this Treatise (Amundson, 2003). In the intervening years, there have been scientific advances and societal changes suggesting that a renaissance of interest in soils is underway, thus providing ample material for this revised chapter.

As a testament to the growing interest in the role of soil in society, it is worth noting that movies are now being made about the topic! (*Dirt! The Movie; The Symphony of Soil, in production*). Students and nonstudents alike are concerned with the sustainability of our food production system and are increasingly exploring the production of their own food. The basis of agriculture is soil. We are now well into the century in which the human population will reach a peak of 9–10 billion people, a trend that will bring with it the need to utilize the potentially arable (and grazeable) landscapes of the planet with even greater intensity, greatly changing the boundary conditions of chemical and physical processes in these soils. In total, humans are taking the center stage as geological agents of soil formation – yet the effect on many chemical processes remains at best obscure. Finally, as we fully exploit our own planet, NASA has become increasingly successful in exploring the soils of our nearest planetary neighbor: Mars. Thus, this chapter will end with a view beyond Earth, one that in some ways reinforces the importance of more fully understanding and maintaining our own planet's soil veneer.

7.1.2 What Is Soil?

Soil is altered surficial rock or sediment. How much, and what type, of alteration distinguishes soil from nonsoil is an ongoing discussion relevant to current research. Some of the differing views are discussed later. However, a key starting point is the work of Jenny (1941). Jenny (1941) applied principles from the physical sciences and defined soils as *systems* (or if the aboveground flora and fauna are considered, *ecosystems*) that exchange mass and energy with their surroundings and whose properties can be defined by a limited set of independent variables:

$$\underbrace{\text{Soils/ecosystems}}_{\text{dependent variables}} = f\underbrace{\left(\begin{array}{l}\text{initial state of system,}\\ \text{surrounding environment,}\\ \text{time}\end{array}\right)}_{\text{independent variables}} \quad [1]$$

The generic independent variables are encompassed by a set of environmental and geological controls that allow the model to be a useful research tool:

$$\text{Soils/ecosystems} = f\left(\underbrace{\text{climate, organisms,}}_{\text{surroundings}}\ \underbrace{\text{topography, parent material, time}\ldots}_{\text{initial state}}\right) \quad [2]$$

Simply stated, soil is the surface material that differs from its parent material in response to processes driven by environmental conditions and the passage of time. Through judicious site (system) selection, the influence of a single factor can be observed and quantified in nature. A field study designed to observe the influence of one state factor is commonly referred to as a *sequence*, for example, a series of sites which have similar state factor values except climate is referred to as a climosequence.

This model has been a valuable tool for soil study and experimental design. Presently, it is serving as the organizing principle behind the Critical Zone Exploration Network (CZEN), a consortium of pedological scientists. One goal of this network is to organize data from published soil studies along sequences of time, climate, lithology, etc., and then use these metadata to better understand general geographical trends in soil processes (**Figure 1**; Banwart et al., 2011). These growing compilations represent a new generation of research that is arranged around the concepts of Jenny. One of the first studies to result from this consortium is that of Rasmussen et al. (2011), which will be discussed later in the chapter. The CZEN effort is also just a small component of the web-based data on soils that are now easily available.

One important conceptual issue about soil is the differing views of soil thickness among differing scientific communities. In the earth sciences, particularly hillslope geomorphology, soil is considered to be restricted to the mobile portion of the weathering profile, where material no longer reflects the fabric of the parent rock or sediment (**Figure 2**; Dethier and Bove, 2011). In many field settings, this largely restricts 'soil' to the A horizons, or biogenically mixed material. In many settings, the B horizons, while exhibiting significant chemical weathering of many types, still maintain enough rock fabric that they are considered *saprolite* (**Figure 2**). This definition is useful for mass balance studies of the production and removal of the mobile soil layer by creep mechanisms (e.g., Heimsath et al., 1997). However, from a geochemical perspective, the separation of soil from saprolite fails to highlight the entirety of the soil formation process, and how geochemical weathering penetrates to considerable depths in the crust – a key process of soil formation. Thus, in this chapter, there is a balance between these two complementary but yet differing concepts of soil.

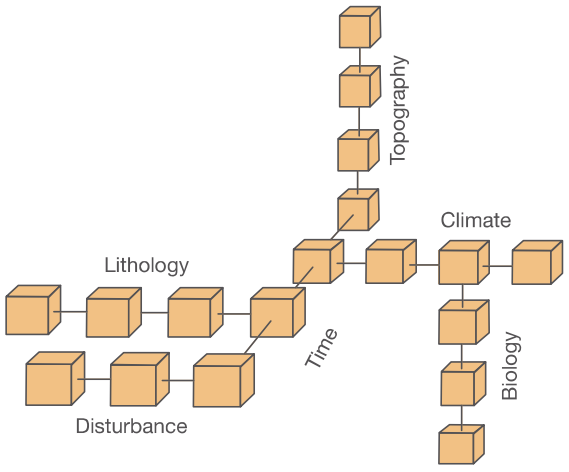

Figure 1 The conceptual linkage between research sites in the CZEN network. The goal of the network is to encourage scientists working on sites along the state factor (eqn [1]) gradients to provide data so that meta-analyses of geographical differences in soil chemistry can be determined (see: http://www.czen.org/) (Courtesy of S. Brantley).

7.1.3 Geographical Access to Soil Data

One of the most remarkable resources to anyone interested in accessing soil data within the USA is the ease of access to a relative wealth of geospatially referenced laboratory data. The Natural Resources Conservation Service (NRCS) is the US federal agency charged with most soil mapping, and subsequent sample analysis and data interpretation for soil survey reports.

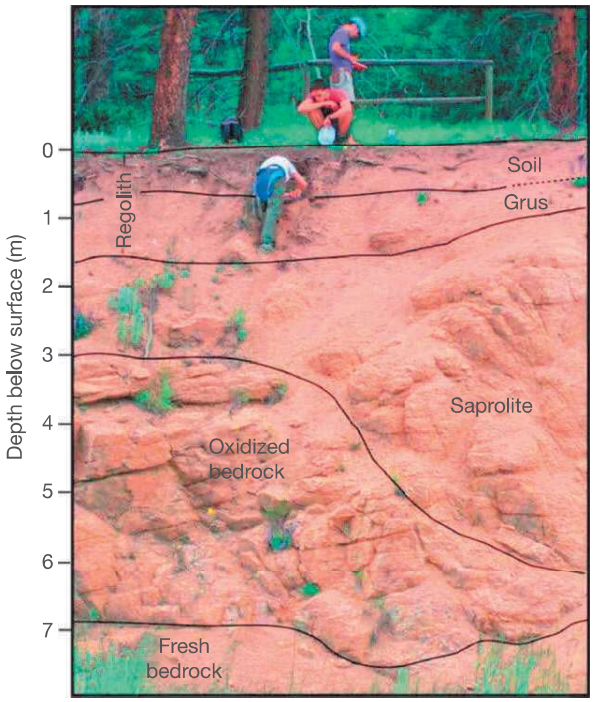

Figure 2 Photograph of a hillslope profile at the Boulder Creek Critical Zone Observatory. The mobile soil layer is separated from underlying physically intact (but chemically weathered) grus and saprolite (reproduced from Dethier DP and Bove DJ (2011) Mineralogical and geochemical changes from alteration of granitic rocks, Boulder Creek catchment, Colorado. *Vadose Zone Journal* 10: 858–866). Gordon Gulch, the midpoint of the Observatory, is located at 40°00′ 31.10″ N, 105°26′ 28.22″ W.

Much of the USA has been mapped at a scale of 1:24 000, and the data are now available online through two different, but complementary, portals.

First, the NRCS has developed the Web Soil Survey, a portal for soil maps and lab data for various soils. While this interface offers unique options such as thematic mapping by soil property, the area that can be evaluated must not exceed 4000 ha, making geographical assessments (presently) somewhat slow and cumbersome. Additionally, soil properties are presented individually. Probably the most useful resource for soil data for earth scientists is the Soil-Web (Beaudette and O'Geen, 2009). Accessing the same database as the Web Soil Survey, it uses a different web architecture allowing interfaces with Google Earth, Google Maps, and with both iPhone and Android smart phones (Beaudette and O'Geen, 2010).

NRCS soil data include the field description of the soil profile characteristics and accompanying laboratory analyses of physical, chemical, and mineralogical properties. The data commonly measured are listed in **Table 1**. Many of the chemical measurements are extractive – providing information on operationally defined mineral abundances or exchangeable phases. More recently, total chemical analyses have been increasingly performed (Burt et al., 2003) and are available through a separate portal at the NRCS web site. Later in this chapter, I use the NRCS database to illustrate the human impacts on soil processes.

While presently the most complete web-based soil database is in the USA, there is a flurry of research and funding to develop similar resources for the globe (Sanchez et al., 2009). The development of this resource will have both scientific and societal benefits, particularly for the improvement of agriculture and the alleviation of poverty. However, since soil survey efforts in the USA have been underway for more than a century (ftp://ftp-fc.sc.egov.usda.gov/NSSC/NCSS/History/1998swcspapers.pdf), there is a need for considerable ground-based study to provide the underlying data needed for this global effort.

Table 1 A summary of the physical and chemical measurements made in a typical soil characterization by the NRCS in the USA

Physical properties
Particle size:
• <2 mm (total sand, silt, clay + subdivisions of each)
• >2 mm (total + subdivisions)
Bulk density
Coefficient of linear extensibility
Water content at differing water potentials
Water holding capacity
Aggregate stability
Atterberg limits
Chemical properties
Organic C, N, S
A series of operationally defined extractions for differing Fe, Al, and Mn – mineralogies
Cation exchange capacity
Base saturation
Exchangeable cations
Water-soluble cations
Electrical conductivity of soil solution
Total salts
pH of soil solution
Carbonate
Gypsum
Operationally defined *P* availability
XRD of both < and >2 μm soil fractions

Some analyses are regional or soil specific, so not all possible measurements are represented. For methods of all NRCS analyses, see the Laboratory Methods Manual (Burt, 2004).

7.1.4 Conceptual Partitioning of the Earth Surface

Soil formation is a process strongly driven by the boundary conditions for the soil system. One of the key conditions (e.g., initial state in eqn [1]) is the physical configuration of the landscape, which dictates the nature of the 'geomorphic surface': the atmosphere/land boundary. From a physical perspective, landscapes can be stable, erosional, or depositional. While physical erosion or deposition can be driven by wind and other processes, slope-driven transport dominates many soil-mantled landscapes. From this perspective, the three landsurfaces can be defined as a function of slope and curvature (the change in slope with downslope distance):

- *Stable Landsurface*: slope $(dz/dx) = 0$;
- *Erosional Landsurface*: curvature $(d(\text{slope})/dx) = (-)$
- *Depositional Landsurface*: curvature $= (+)$

Figure 3 illustrates this very general landscape partitioning. This partitioning is idealized. Mass can be gained or lost from all parts of the land surface by a variety of processes. However, these categories identify some useful starting points for discussion. Each of these physical environments sets unique boundary conditions for soil formation and its biogeochemical processes. I begin here by focusing on stable landsurfaces.

7.1.4.1 Stable Landforms

Total chemical analyses of soils, when compared to parent material, provide unambiguous insights into quantitative gains and losses with depth (see **Chapter 7.4**). While this has long been known (Merrill, 1906), the approach experienced a reemergence with publications by Brimhall and Dietrich (1987) and Brimhall et al. (1992). Briefly, gains or losses of an element (or total mass) in a soil layer relative to the soil's

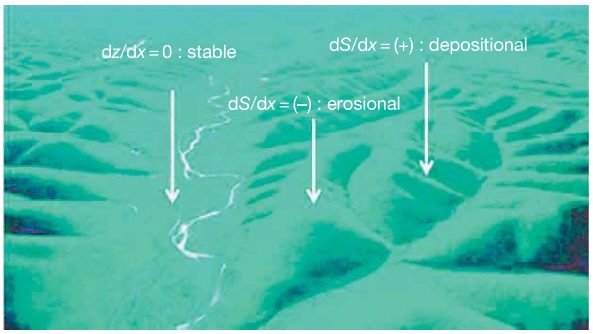

Figure 3 A very simple classification of the three key physical soil-forming environments on the basis of landsurface stability (reproduced from Dietrich WE and Perron JT (2006) The search for a topographic signature of life. *Nature* 439: 411–418). S = slope = (dz/dx), z = vertical distance, and x = horizontal distance.

parent material can be established by normalizing the content of that element (e.g., Na) relative to an element that is essentially immobile in the soil weathering environment. Commonly used immobile elements (Zr, Ti, Nb, etc.) tend to lie in groups 4 and 5 of the periodic table, (Railsback, 2003; Figure 4). Gains or loss is reported as fractions or *tau values*:

$$\tau = \frac{c_{m,s}/c_{i,s}}{c_{m,p}/c_{i,p}} - 1 \qquad [3]$$

where c is the concentration of a mobile (m) or immobile (i) element in the soil (s) or parent material (p). The total mass gain or loss for an entire soil (to some chosen depth or for the entire depth of weathering) is the integration of all layers to a chosen depth, or to the parent material. To calculate volumetric change, the following expression is commonly used:

$$\varepsilon = \frac{\rho_p C_{i,p}}{\rho_s C_{i,s}} - 1 \qquad [4]$$

where ε is the fraction volume change of a horizon (or a whole soil if volume change for all horizons is summed over the distance of interest) and ρ is the bulk density (g cm^{-3}) of the soil or parent material.

Because soil formation is a process that occurs over millennia, the most instructive way to investigate it has been through the establishment of research sites on stable landforms of increasing age – studies called *chronosequences*. The morphological and chemical analyses of these sequences reveal some nearly universal processes that underlie soil development.

In Amundson (2003), I examined how soils change with time. Here, I approach this process again, but illustrate it in more, and differing, detail. The sequence chosen to begin the discussion contains the soils found on terraces of the rivers draining the western flank of the Sierra Nevada range in central California (Figure 5). The geologic setting is detailed in Harden (1987), and the best age constraints are provided by Pavich et al. (1986). The chronosequence is located on terrace and fan deposits of the Merced and Tuolomne rivers, which drain the western slope of the Sierra Nevada and descend into the San Joaquin Valley. Cyclic episodes of glaciation of the Sierra Nevada during the Pleistocene, combined with tectonic uplift of the mountain range, resulted in rapid deposition events (after glacial melting) that are followed by stream entrenchment and subsequent periods of slow sedimentation (Harden, 1987). Old alluvial fans that opened to the west have been incised over time by the cyclic erosional/depositional events and now contain a suite of inset river terraces. Soils and ecosystems found on the complete sequence of these terraces comprise a chronosequence varying from Holocene ($\sim 10^2$ years) to Plio–Pleistocene ($\sim$3000 ky) in age. Here, I

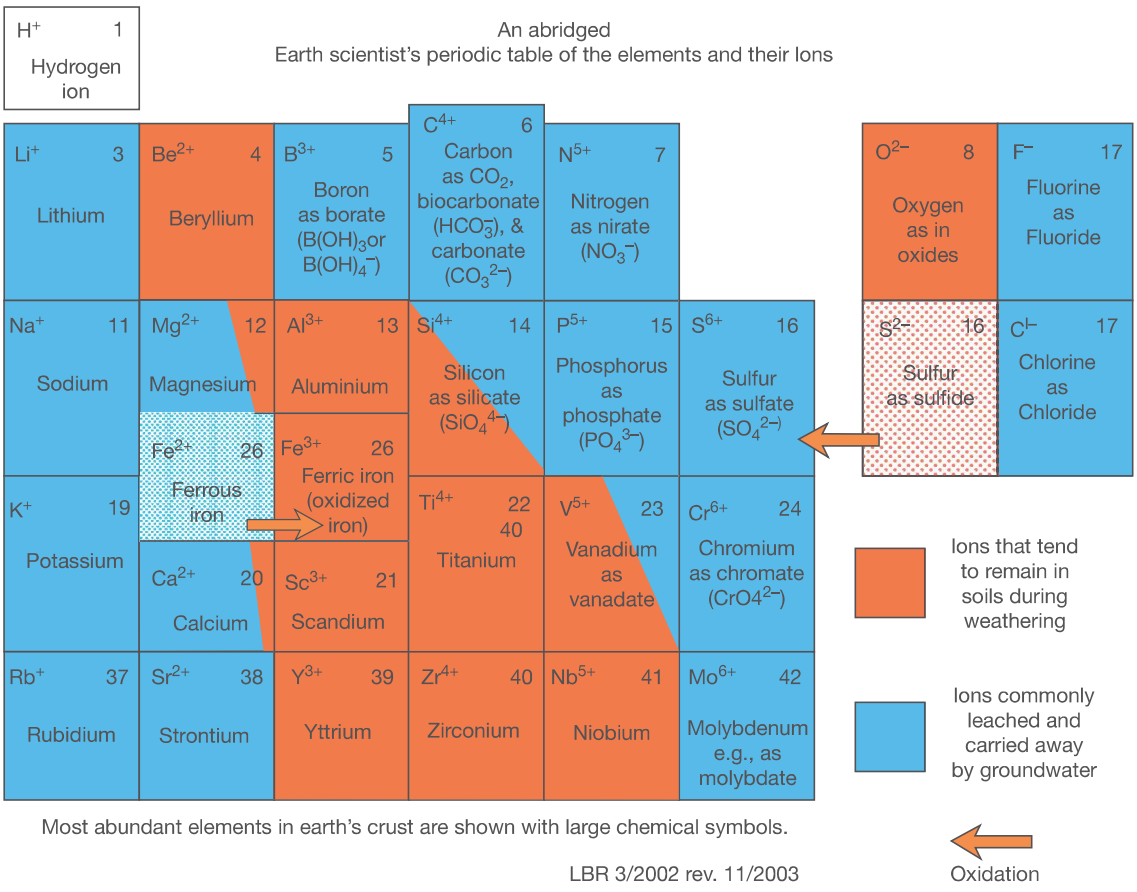

Figure 4 An abridged periodic table, showing some of the key soil-forming elements and their relative behavior during weathering (reproduced from Railsback BL (2003) An Earth scientist's periodic table of the elements and their ions. *Geology* 31: 737–740. (http://www.gly.uga.edu/railsback/PT.html)).

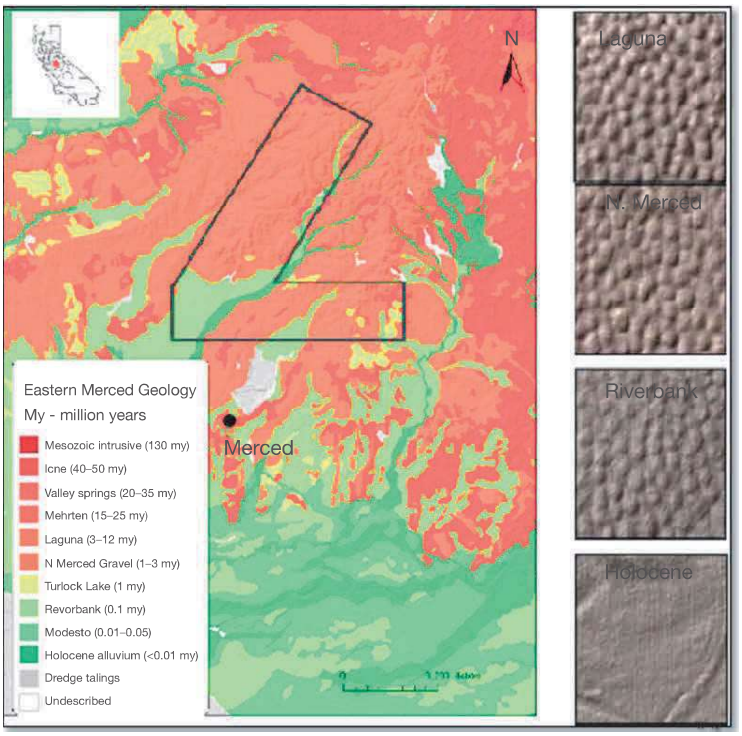

Figure 5 Colored relief map of the Stanislaus and Merced River drainages, and the high elevation Sierra Nevada Range to the east. The panels on the right show the Lidar-based view of the changes in surface topography of the terraces due to Mima mound formation: lowest panel = youngest, upper panel = oldest, landforms.

use data from Harden (1987) to illustrate some key principles of soil formation.

Figure 6 shows a schematic representation of how the soil profiles change as a function of age. The diagram reveals a number of important principles that apply to a majority of soil formation environments:

- Initial stages of soil development are dominated by organic matter additions. Because organic matter is not rock derived, mass is added to the soil from atmospheric sources fixed by photosynthesis: CO_2 is fixed to carbohydrates and NO_3 and NH_4 are fixed within amino acids. Along with the impact of root and biota mixing of soil, the soil undergoes modest expansion (**Figure 6(b)**). In more humid environments, the expansion is more pronounced due to greater organic accumulation and to the production of hydrated mineral phases (e.g., the addition of water to total mass and volume) (e.g., Brimhall et al., 1992). In the Merced River region, the bulk density decrease of the original river sediment ($\sim$1.4 g cm^{-3}) is the driving mechanism behind the small volumetric expansion early in soil development.
- Initial thickening of soil (the removal of rock or sediment structure) proceeds largely via biotic mechanisms which physically disrupt sedimentary structure. Accompanying this physical mixing is a slight reddening of subsurface soil colors (distinct visible identification on time scales of $\sim 10^3$ to 10^4 years). At Merced, the visual oxidation is correlative with an increasing ratio of citrate-dithionate extractable Fe/oxalate extractable Fe ($\sim$(goethite+hematite)/ferrihydrite) ratios.
- The next identifiable pedogenic change is the accumulation of secondary clay minerals (<2 μm particles) in the B horizons, beginning at $\sim$40 ka (**Figure 6(a)**). These are the weathering products of the breakdown of the primary minerals (White et al., 1996; **Figure 6(b)**). Soil thickening continues with time.
- Clay accumulation and soil thickening continue with increasing soil age. Corresponding to clay accumulation, volume is lost through weathering and through increased bulk density (**Figure 6(b)**) (as clay fills in the porous nature of the initially sandy alluvium). Volumetric collapse thus proceeds with the passage of time. A combined perspective of average soil volume change and mass loss with time is illustrated in **Figure 6(b)**.

From a geomorphic perspective, the 'soil' (mobile layer) in these soils – particularly the oldest profiles – is the A horizons, which are $\sim$the upper 30–50 cm. The driving force behind this mobilization of particles is a combination of root penetration by plants and burrowing insects and animals – especially gophers (*Thomomys bottae*) and ground squirrels (*Spermophilinus* sp.) (Reed and Amundson, 2007, 2012). The depth of burrowing and soil mixing is commonly delineated by both a rapid change in color (from dark humus-rich A horizons to oxidized B horizons) and the presence of a stone or gravel layer at the base of the mixing zone (**Figure 7**). The increase in clay with time decreases hydraulic conductivity and increases near-surface soil saturation during winter precipitation, and as a result burrowing organisms appear to have accomplished directional soil movement with time, creating a distinctive 'mound and swale' topography, one

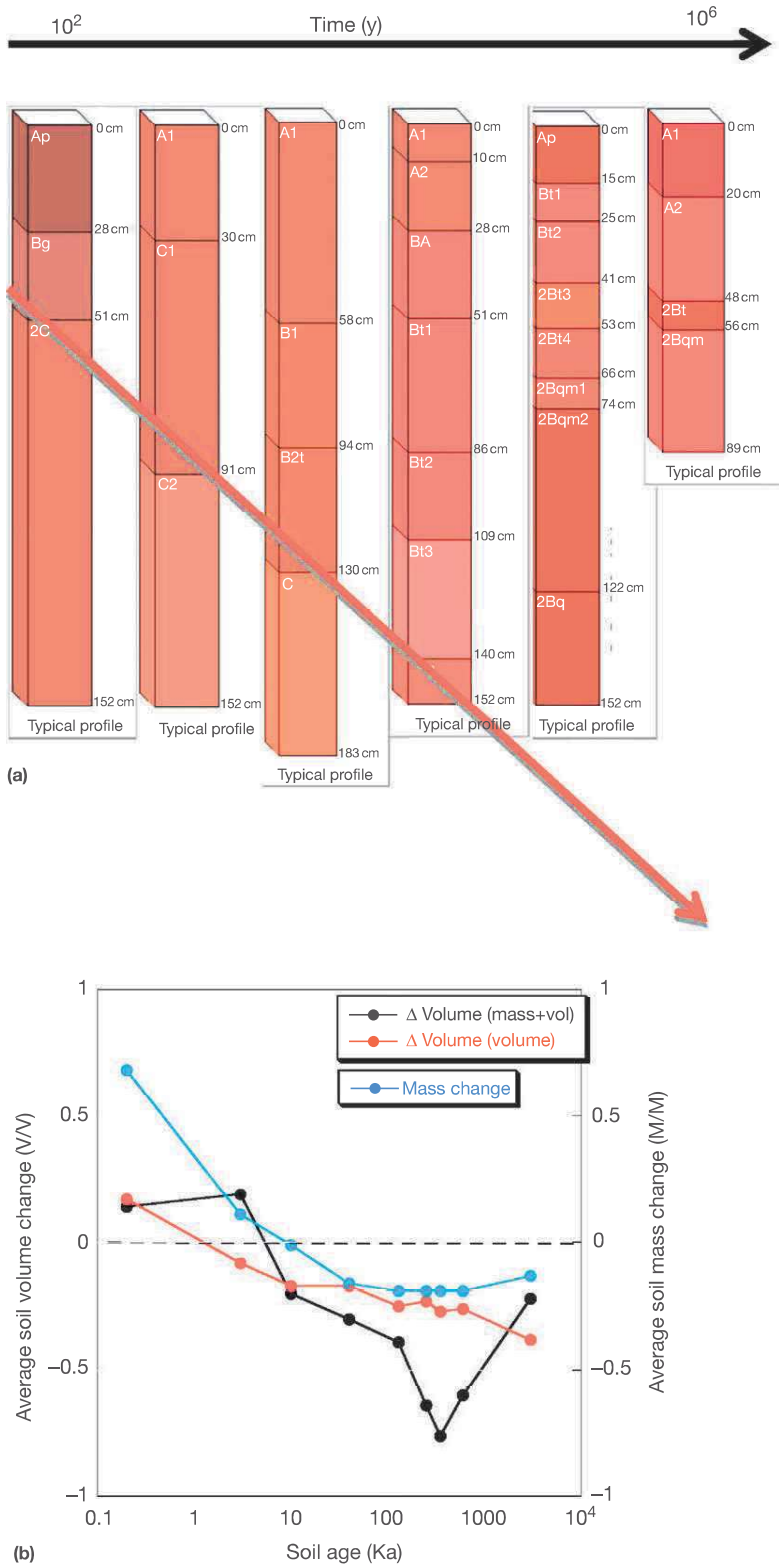

Figure 6 (a) Schematic representation of the San Joaquin Valley soil chronosequence, with the red arrow approximating the change in the depth of the C horizon (unweathered sediment) with time (b) tau and volume change with time. Volume change is calculated from bulk density changes with time (volume) and combined mass and bulk density changes. Images in (a) from Soil-Web. Soil data for (b) from Harden (1987).

Figure 7 A typical California annual grassland soil profile, showing the dark A horizon (the biomixed layer), the underlying stone line, and the B horizon below the stone line (highly weathered but physically unexpanded saprolite). Photograph by R. Amundson.

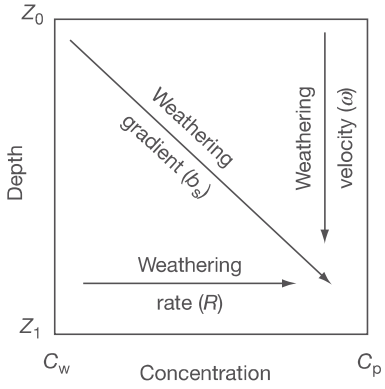

Figure 8 A representation of the relationship between weathering rate, the weathering front velocity, and the resulting weathering gradient in soils. Reproduced from White AF (2002) Determining mineral weathering rates based on solid and solute weathering gradients and velocities: Application to biotite weathering in saprolites. *Chemical Geology* 190: 69–89.

that progressively increases in prominence with soil age (**Figure 5**). While this bioturbation effect is particularly accentuated on the ancient terrace soils, this is a universal process in California and many other locations (Johnson, 1990), explaining as Darwin (1881) illustrated, why the artifacts of human occupation soon lie buried beneath soil particles lofted upwards by worms, insects, and animals.

In the past decade, considerable work has been devoted to interpreting observed solute, and solid, soil chemistry profiles (see **Chapter 7.4**). There have been complementary approaches from the solution phase perspective (e.g., Maher, 2010; Maher et al., 2009) and from the solid phase (e.g., Brantley and Lebedeva, 2011; Brantley et al., 2008; White, 2002; Williams et al., 2010). Here, just a brief overview of this work is presented in order to provide an introduction to a growing tool kit allowing geochemists to 'read soil profiles' (Brantley and Lebedeva, 2011) with greater clarity and insight.

Studies of the geochemistry of soils along gradients of age or climate reveal systematic changes in the depth profiles of mobile elements. As water moves into soils and combines with CO_2 and other biologically mediated acids, it reacts with primary minerals until chemical equilibrium with a controlling phase is reached. In general, the solid and solution phase *weathering gradient* (dC/dz), the increase in the concentration of a mobile element with depth (to the parent material value (solid) or equilibrium value (solution)), is driven by the balance between the weathering rate (R) and fluid velocity (q) (**Figure 8**). The reaction rate (R_d) is driven by the kinetic rate constant for a mineral (k), the effective surface area (A), and the distance from chemical equilibrium (Q/K_{eq}) (Maher, 2010):

$$R_d = -kA\left(1 - \frac{Q}{K_{eq}}\right) \qquad [5]$$

The weathering gradient is proportional to the reaction rate and inversely proportional to water flow rate (q)($l\ ton^{-1}$) (Maher, 2010):

$$\frac{dC}{dz} = \frac{R_d}{q}\left(1 - \frac{c}{c_{eq}}\right) = \frac{c_{eq} - c_0}{L_e} \qquad [6]$$

where c = initial fluid concentration (0), measured, or equilibrium (eq). The term L_e is the thickness of the weathering reaction front in the soil, or the distance required for downward moving fluids to reach chemical equilibrium. Increasing flow (at a given weathering rate) reduces the gradient, while increased weathering rate (at a constant flow) increases the gradient. For soil profiles at steady state, the rate at which the weathering front moves downward (ω) is approximated by (Brantley et al., 2008; Maher, 2010; White et al., 2008):

$$\omega = \frac{qc_{eq}}{C_0} \qquad [7]$$

where C_0 = concentration of a mineral in the parent material.

One important point that emerges from this ongoing research is that except for initial transient states, nearly all soils are *transport limited* in the sense that the flow of fluid, rather than rates of mineral dissolution, is the limiting factor to chemical dissolution in the profile (Maher, 2010). Only for extraordinary (and likely unrealistic) amounts of precipitation soils would actually become *weathering limited*. For a given mineral weathering rate, the length over which the weathering occurs (L_e), and the corresponding slope of the weathering front, is dependent on fluid flow. Maher (2010), using the reaction transport model CrunchFlow (Steefel and Lasaga, 1994), calculated the movement of a feldspar weathering front through a soil similar to that on marine terraces at Santa Cruz, CA (White et al., 2008; **Figure 9**). Precipitation (and its related soil parameter fluid flow, q) determines the rate at which the weathering front advances through a soil, and the depth it will be found at some given point in time. Increases in the weathering rate constants alter the gradient but do not alter the weathering front position.

One of the key points of this research is that rates of weathering can remain constant with time as the weathering front

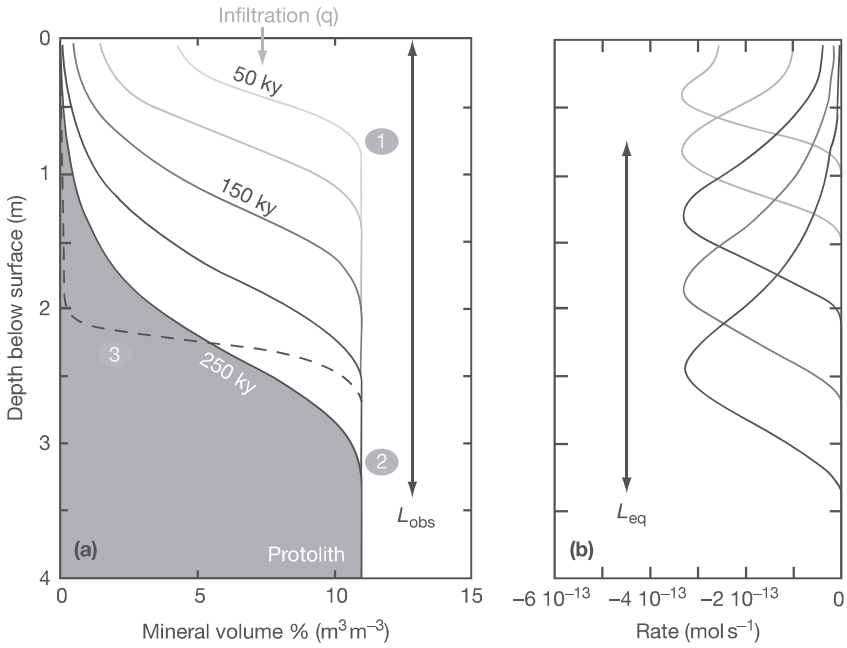

Figure 9 (a) Schematic of transport-controlled weathering showing the evolution of feldspar abundance over time and as a function of depth and (b) the corresponding bulk reaction rates (mol l^{-1}(porous media) s^{-1}) as a function of depth for the profiles in (a). L_{obs} corresponds to the observed weathering length scale at the time of measurement (250 ky). L_{eq} corresponds to the distance over which the fluid equilibrates with the solid and reflects the zone where weathering is occurring. Points on the profiles correspond to key features of transport-controlled weathering. (1) Nonsteady-state profile evolution where mineral abundance at the top of the profile has not yet been depleted; (2) steady state profile evolution where mineral at the top of profile has been mostly depleted and the rate of profile advance becomes constant; and (3) an order of magnitude increase in the mineral surface area or kinetic rate constant sharpens the profile but does not appreciably change the mass of material removed due to weathering. Reproduced from Figure 1 of Maher K (2010) The dependence of chemical weathering rates on fluid residence time. *Earth and Planetary Science Letters* 294: 101–110.

advances deeper and deeper into the soil profile (Maher, 2010). Therefore, one of the practical challenges for soil research in old and/or humid landscapes is sampling deeply enough to capture the weathering profile. Many or most typical soil excavations are on the order of 1–2 m, and in these observations the weathering front may have already passed through, and therefore the nature of its chemical composition (either solid or aqueous) gives little insight into the processes occurring at greater depths. Thus, it is important in soil research to make deep sampling a priority.

Brantley et al. (2008) devised models to extract potential kinetic and energetic information from solid phase chemistry of soils – data which are more commonly available than solution phase chemistry. Here, their analysis of Holocene loess soil profiles along a north to south temperature gradient in the central USA (**Figure 10(a)**) is reviewed. In those soils, the loss of the mobile element Na increased with increasing temperature (**Figure 10(b)**). However, since the Na had not been completely depleted from the surface of any of the soils, it was assumed that the weathering fronts had not reached steady state in any soil, and thus all were still kinetically limited weathering situations. Thus, the authors used these relations to extract the in situ temperature dependence of weathering rates from the profiles. Using measured values of the parent material Na concentration (C_0) and the concentration at some depth z (C), the authors used the following equation to extract a 'lumped' kinetic parameter K (m^{-1}) for each soil:

$$C = \frac{C_0}{(C_0 - C_{z=0}/C_{z=0})\exp(-K \times z) + 1} \quad [8]$$

The lumped K parameter is equal to:

$$K = \frac{kA\Gamma\gamma}{\upsilon\beta} \quad [9]$$

where k = rate constant for mineral dissolution (mol m^{-2} s^{-1}), A = geometric surface area of dissolving mineral grains (m^{-2}), Γ = roughness of parent grains (dimensionless), γ = an activity correction term, υ = velocity of pore fluid flow (m s^{-1}), and β is a dimensionless buffer capacity term. Williams et al. (2010) assumed activity was unity, that buffering and surface area characteristics were nearly constant between soils, so that the product of (Kv) was considered proportional to changes in k. The relationship:

$$\ln k = \ln A' - E_a/RT$$

links changes in k to E_a = the apparent activation energy of mineral dissolution and A' a pre-exponential factor. By plotting $\ln k$ (or Kv) versus $1/T$ for the data from these sites, the authors calculated the activation energy of the albite weathering

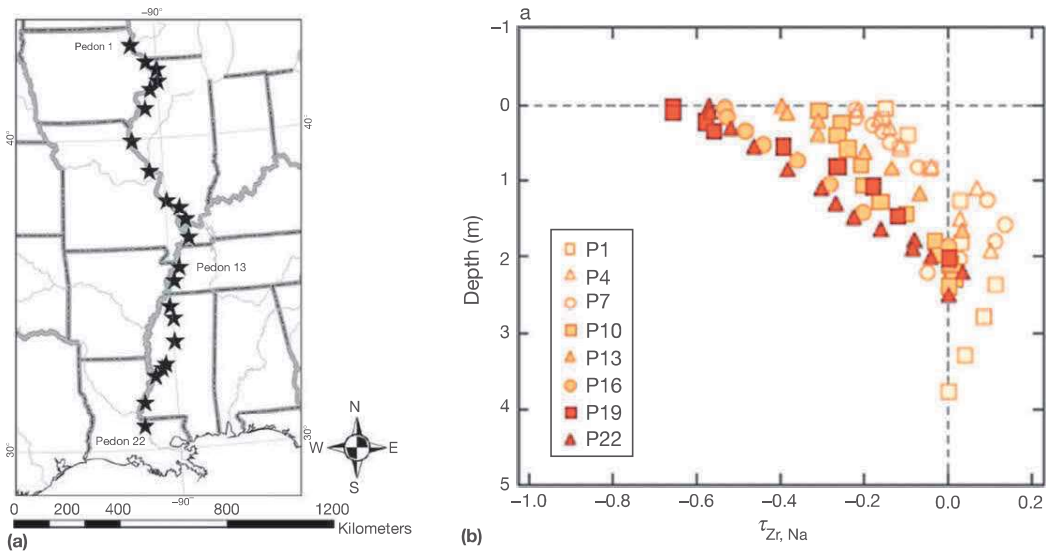

Figure 10 (a) Soils in Holocene loess by latitude (Williams et al., 2010) and (b) calculated fractional losses of Na (Brantley and Lebedeva, 2011).

reaction to be between 93 and 182 kJ mol^{-1}, values within the range reported from laboratory studies.

These examples focus on highly soluble elements and the corresponding characteristic depletion profiles that develop. However, during soil formation, secondary mineral precipitation, particularly of Al and Fe silicates or oxides, also occurs. Maher et al. (2009) show that along a chronosequence of soils on marine terraces on the California central coast (White et al., 2008), the positioning of the clay-rich B horizons could be explained almost entirely by in situ precipitation of kaolinite as the downward migrating fluids passed from kaolinite undersaturation, to saturation, with increasing depth. The precipitation of the kaolinite in turn serves as an elemental sink for Al and Si, controlling the rate of weathering front propogation and the total mass lost from the soil. Maher et al. (2009) suggested that secondary mineral formation is as important as aqueous transport in controlling primary mineral weathering rates.

This research on stable landscapes is also important, as will be discussed, in understanding soil chemistry on erosional landforms.

7.1.4.2 Erosional Landscapes

One of the most important conceptual changes in the view of soil formation in the past 15 years has been the adoption of the process-based model of soil production and transport on soil-mantled hillslopes (for a review, see Dietrich et al., 2003). This is a physical model that relies on quantitative geochemically derived rates of landscape denudation using one of the several cosmogenically produced isotopes (see **Chapter 7.12**). Initially, soil production and transport was largely viewed, for simplicity, as a purely physical process, and chemical gains and losses were implicitly ignored. This simplification was overcome by the work of Riebe et al. (2001) (discussed below), and now geochemistry is becoming increasingly coupled with geophysics as the dynamics of upland soils are deciphered.

Riebe et al. (2001) combined physical and chemical processes on hillslope soils. Briefly,

$$W = D - E = D\left(1 - \frac{C_{i,p}}{C_{i,s}}\right) \quad [10]$$

where W=chemical weathering rate, D=cosmogenically derived total denudation rate, $C_{i,p}$ and $C_{i,s}$=the concentration of an immobile element (i) in the parent material (p) and soil (s), and E=physical erosion rate. Thus, from cosmogenic denudation measurements and soil and parent material chemical analyses, the chemical weathering rate can be determined. Rearranging eqn [10] yields a term called the chemical depletion factor (CDF) (Riebe et al., 2004), which is the relative contribution of chemical erosion to total denudation.

$$\mathrm{CDF} = \frac{W}{D} = \left(1 - \frac{C_{i,p}}{C_{i,s}}\right) \quad [11]$$

This model implicitly assumes that all material replacing soil is derived from the underlying saprolite/bedrock. Additionally, it is assumed that the time for chemical weathering (the soil residence time) is the mass of the soil divided by the soil production rate (in mass $time^{-1}$). These assumptions are valid for soils found at hillslope summits, where inputs of soil from upslope positions do not occur. However, in other slope positions there is an influx of material into a given soil box by creep from upslope positions, which should add preweathered material from upslope and should decrease the effective soil residence time. This simplification was recognized, and to circumvent the effect of lateral movement, soils sampled on hillslope crests can be rigorously examined using these relations (e.g., Rasmussen et al., 2011).

In order to examine soils along a slope transect (which are areas subject to lateral soil creep), Yoo et al. (2007) developed a framework amenable to describing these combined processes (**Figure 11**). Weathering can be partitioned into two components, weathering of saprolite-derived soil particles (W_ϕ) and weathering of laterally transported material (W_s):

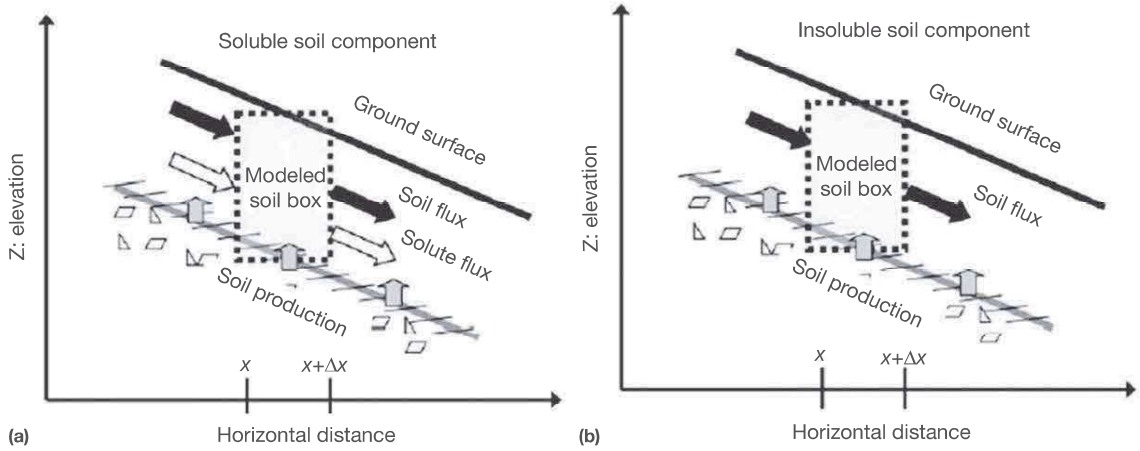

Figure 11 Conceptual model of (a) the behavior of water-soluble elements and (b) insoluble elements on soil-mantled hillslopes. Reproduced from Yoo K, Amundson R, Heimsath AM, Dietrich WE, and Brimhall GH (2007) Integration of geochemical mass balance with sediment transport to calculate rates of soil chemical weathering and transport on hillslopes. *Journal of Geophysical Research* 112: F02013.

$$W = \underbrace{\left(1 - \frac{C_{i,p}}{C_{i,s}}\right)\phi}_{W_\phi} + \underbrace{\frac{\nabla C_{i,s}}{C_{i,s}}\tilde{Q}_s}_{W_s} \qquad [12]$$

where $\tilde{Q}_s$ = soil flux$(\mathrm{ml}^{-1}\mathrm{ton}^{-1})$. Similarly, soil residence time on slopes has two components: (1) the first from soil production from underlying saprolite (a vertical flux of material displacing soil material, $T_R\uparrow$) (the residence time commonly calculated using denudation rates) and (2) a lateral component ($T_R\rightarrow$) due to soil creep:

$$T_R\uparrow = \left(\frac{\rho_s C_{i,s} h_s}{C_{i,p}\phi}\right) \qquad [13]$$

and

$$T_R\rightarrow = \frac{\rho_s C_{i,s\_x+\Delta x} h \Delta x}{C_{i,s\_x} Q_{s_x}} \qquad [14]$$

Yoo et al. (2007) developed an iterative, numerical spreadsheet model that uses measured soil and saprolite chemistry along a slope gradient, along with soil production rates, to simultaneously calculate both weathering rates and soil flux (assuming the system is at steady state). By applying this approach to a transect of soils along a downslope gradient at Frogs Hollow, Australia (**Figure 12(a)**), the analysis revealed some very interesting slope-driven processes:

- The integrated soil weathering rates declined downslope, and actually reversed to net gains near the slope toe (**Figure 12(b)**).
- If weathering had been based on a comparison to saprolite only (W_ϕ), a net weathering loss would be interpreted along the entire slope transect.
- As might be expected, there is a dramatic reduction in soil residence time if lateral transport of particles is considered, reducing soil profile residence times from $\sim 10^4$ to 10^3 years depending on slope position (**Figure 12(c)**).

This approach, while requiring a well-conceived sampling plan and corresponding soil production data, allows a quantitative view of both chemical and physical processes along the toposequences (sometimes called *catenas*), transects that have been of interest for decades, but which lacked the soil production data now available from cosmogenic radionuclides (Granger and Riebe, 2007) and a mathematical framework for data analysis.

From the previous section, we know that weathering front propagation rate is largely driven by the rate of fluid movement through a rock/sediment profile (Maher, 2010; White, 2002). The observed depth of a propagation front on eroding hillslopes should therefore depend on the propagation rate and the denudation rate (e.g., soil replacement rate). If denudation rates exceed the propagation rate, the depth of observed chemical depletion in the soil and the underlying saprolite will be shallow. If propagation exceeds denudation, then weathering profiles even on actively eroding slopes should be deep.

Rates of denudation of soil-mantled hillslopes (measured as the *soil production rate*) are largely insensitive to rainfall over a large range in precipitation (**Figure 13(a)**). While the reasons for this are not clear, this correlates with a similar narrow range in soil thicknesses (**Figure 13(b)**). There is an active feedback between soil thickness and soil production and erosion. Although various formulations of this process have been made, the following relationship illustrates the complexity of the feedbacks:

$$\frac{dH}{dt} = P_0 e^{-kH} - K_h H \nabla_z \qquad [15]$$

where H = soil thickness, k = a constant $(1/H)$, P_0 = soil production $(\mathrm{l\ ton}^{-1})$ at 0 soil thickness, K = a diffusion-like constant $(\mathrm{l}^{-2}\ \mathrm{ton}^{-1})$, and the operator ∇_z = curvature. The first term on the right is depth-dependent soil production, and the second is depth-dependent soil removal. The feedbacks between thickness/production/erosion on soil covered hillslopes appear to modulate rates of overall denudation as long as a minimum plant cover is maintained (Amundson et al., 2010). In contrast to the apparent denudation insensitivity to rainfall, weathering front propagation is strongly linked to rainfall and the amount of water available to advect through the soil profile (Maher, 2010). The rate of advance is mineral specific (given differences in dissolution kinetics and

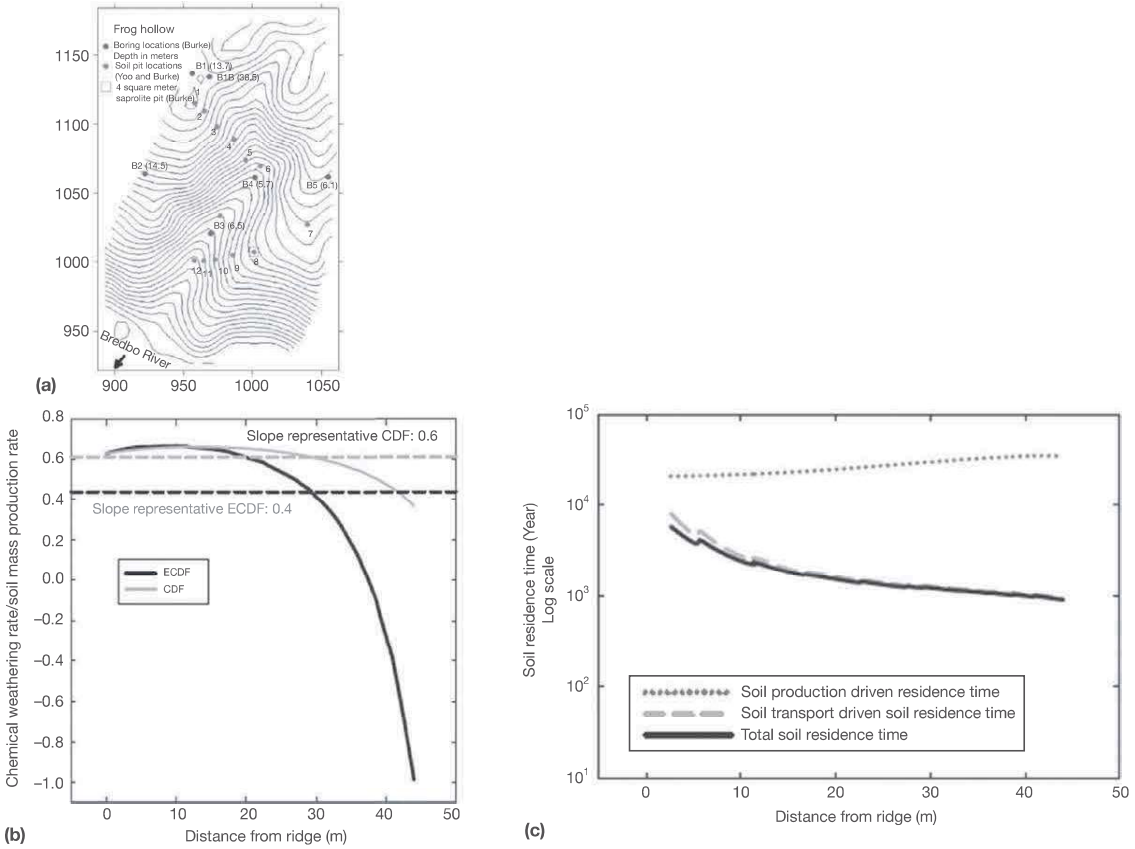

Figure 12 (a) Location of sites along a hillslope in Australia, (b) calculated weathering rates versus distance downslope, and (c) the residence time of the soils assuming all production is from saprolite (soil production driven residence time) or from combined vertical and lateral sources of soil particles (total soil residence time). In panel (b), the ECDF is chemical depletion that accounts for both lateral and vertical fluxes of sediment (as opposed to only a vertical flux assumed for the CDF (eqn [11])). The negative weathering fluxes obtained for the ECDF illustrate that net gains of mass are accumulating in the lower segments of the hillslope from material derived from upslope positions. (a) Reproduced from Burke BC, Heimsath AM, Dixon JL, Chappell J, and Yoo K (2009) Weathering the escarpment: Chemical and physical rates and processes, southeastern Australia. *Earth Surface Processes and Landforms* 34: 768–785); (b and c) Yoo K, Amundson R, Heimsath AM, Dietrich WE, and Brimhall GH (2007) Integration of geochemical mass balance with sediment transport to calculate rates of soil chemical weathering and transport on hillslopes. *Journal of Geophysical Research* 112: F02013.

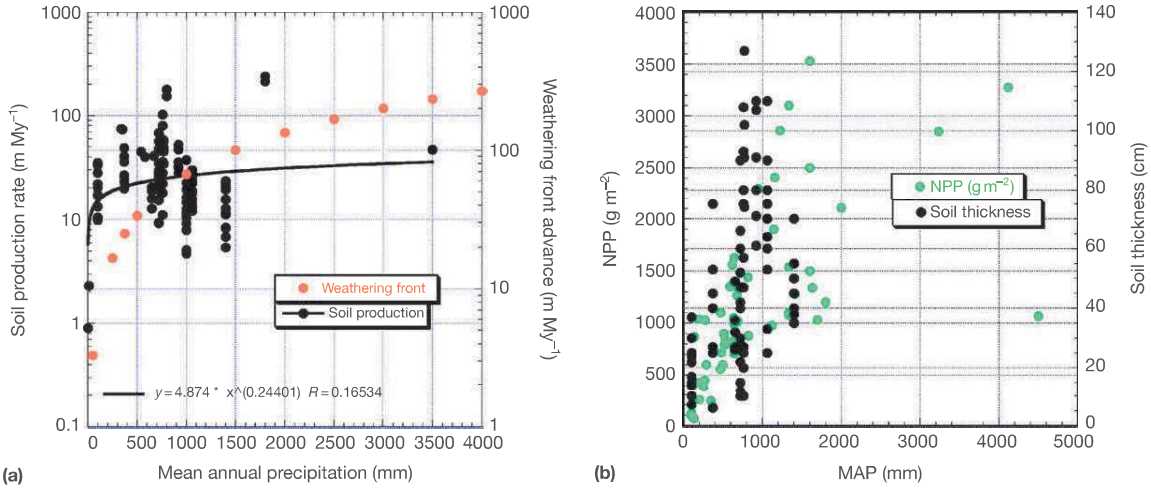

Figure 13 (a) Soil production rate and approximate weathering front thickness versus MAP and (b) soil thickness and net primary production (NPP), a proxy for plant cover, versus MAP (data compiled by Owen et al., 2011 and discussed in Amundson et al., 2010). The weathering front advance in (a) is an approximate rate for albite using data from White et al. (2008).

equilibrium solubilities) and also sensitive to other variables such as CO_2, organic and inorganic acids, etc. Using eqn [7], White et al. (2008) estimated a weathering front advance of ~0.03–0.04 m ky^{-1} for the marine terrace soils near Santa Cruz, CA. Using this relationship, it is possible to make a crude approximation of how wetting front advance rate changes with MAP (**Figure 13(a)**). In the calculation it was assumed that pore water fluid fluxes are 1/5 that of MAP, a value intermediate to that of the global value of 1/3, and the 1/7 found for Santa Cruz (White et al., 2008).

These data, plotted along with denudation vs. rainfall, suggest that above 1.5–2 m of precipitation, weathering propagation should exceed denudation rates. To test this prediction, I use the data recently compiled and analyzed by Rasmussen et al. (2011). These authors assembled soil, saprolite, and bedrock Na and Ti/Zr concentrations, depth, and physical erosion rates for a series of erosional upland settings with wide ranges in denudation and climate (e.g., part of the CZEN effort to analyze metadata). Here I use the data to address two questions not examined in the original paper, but connected to the hypothesis that soil chemical composition on eroding landscapes is a balance between weathering front advance and denudation rates:

1. Does the plot of τ_{Na} (see eqn [3]) of the soil surface (which will reflect the degree of weathering front alteration) versus the ratio of weathering front advance (ω)/cosmogenically derived denudation rate (D) produce a relationship?
2. Does the depth of the weathering front versus ω/D also produce a systematic relationship?

Figure 14(a) shows τ_{Na} of the surface versus ω/D. τ_{Na} increases roughly with ω/D to values of about 2, at which point soil surfaces are depleted of all Na. Even given the approximate nature of the weathering front advance model used here (which essentially is a linear modification of precipitation rate), the results are what would be expected: at drier sites, weathering rates are slow relative to denudation, and chemical weathering is unable to maintain pace with mineral removal. Above a critical ω/D, weathering advance is faster than D, and soil surfaces are entirely depleted of Na even in the face of ongoing denudation.

Figure 14(b) shows the relationship of depth of the weathering front (the depth below which there is a large increase in Na concentration) versus ω/D. The few sites with all the required measurements form a remarkably good relationship, as would be expected if weathering advance rates begin to greatly exceed that of denudation.

These two figures illustrate a few important advances in our understanding of soil formation. First, the development of community-based data for meta-analyses (from individual studies involving considerable time and finances) allows scientists to address complex hypotheses. Second, the merger of process-based geomorphology with process-based soil chemistry appears to offer a much richer perspective on the evolution of landscapes, and ultimately (as discussed below), landscape response to human activities.

7.1.5 The Human Dimension of Soil Formation

All of the research reviewed above was conducted on 'natural' landscapes. One of the ironies that accompanies our rapidly evolving understanding of how these landscapes function is that as this work proceeds, the majority of the planet is being transformed by a geological cataclysm known as 'human beings' (Crutzen, 2002). While it certainly can be argued that the geochemical research on natural landscapes is societally important and will provide a quantitative baseline evaluating human induced change, there is a serious need to launch a more concerted effort to begin quantifying the numerous ways in which humans are altering the earth's surface.

To begin to appreciate the magnitude of human manipulation of soil, our ability to design and manufacture tools has given humans the ability to physically disrupt and modify the immediate land surface of the planet. The global area of cultivated land is ~15×10^6 km^2 (Monfreda et al., 2008; **Figure 15**).

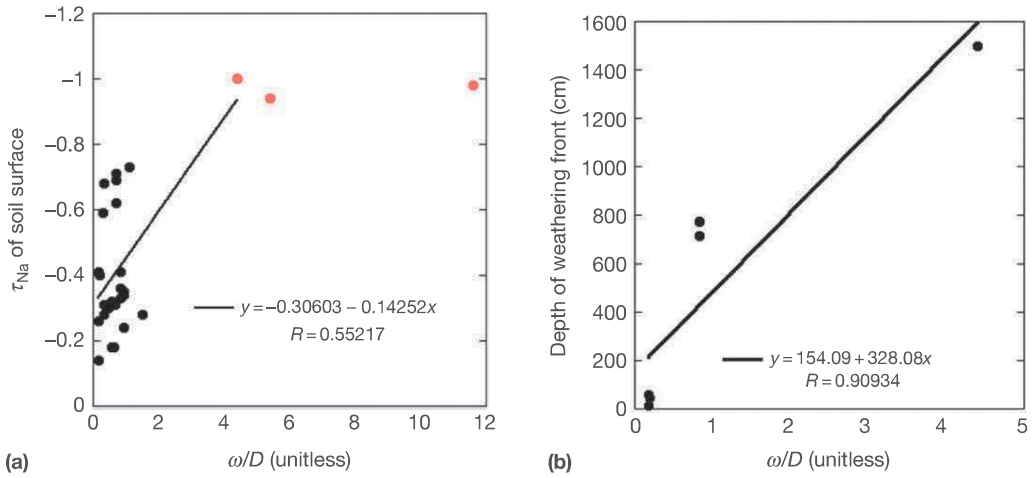

Figure 14 (a) The fractional loss of Na from the surface horizon of upland granitic soils and (b) the depth of the weathering front vs. the ratio of weathering front advance/cosmogenically produced denudation rates. Data compiled by Rasmussen et al. (2011). The black line in (a) is a linear fit through data. The red points illustrate what appears to be sites that lie beyond a critical ratio.

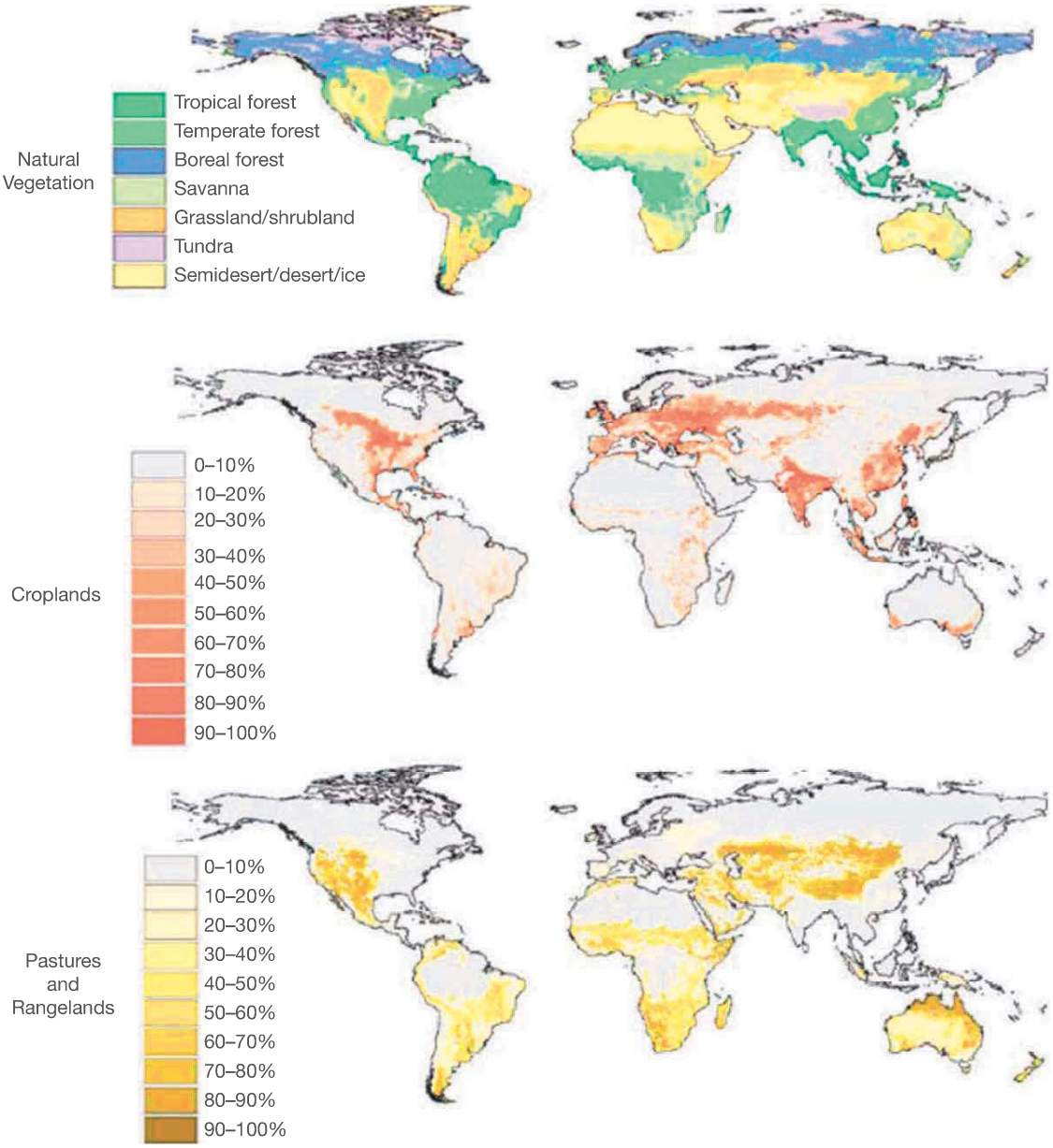

Figure 15 The distribution of natural ecosystems and the extent of agricultural and grazing land use (reproduced from Foley JA, DeFries R, Asner GP, et al. (2005) Global consequences of land use. *Science* 309: 570–574.)

For comparison, the land covered by ice was about $20 \times 10^6\ \mathrm{km}^{-2}$ at the Last Glacial Maximum. Unlike glacial processes, the human sculpting of the surface has largely occurred in the past few centuries. The removal of natural vegetative cover changes the underlying mechanisms of soil transport on hillslopes from slow, biogenic creep to advective overland flow. The increase in landscape denudation rates caused by this mechanistic change is enormous. Figure 16 illustrates soil erosion rates in the USA prior to European settlement and today. The economic and agricultural consequences of this accelerated erosion inspired a mid-twentieth century soil conservation movement in the USA. However, at that time the rates of soil formation processes recently measured in natural landscapes were unknown, or impossible to determine with techniques then available. On a soil-mantled hillslope, soil thickness (H) is the balance between erosion (E (l ton^{-1})) and soil production (P (l ton^{-1})):

$$\frac{\mathrm{d}H}{\mathrm{d}t} = P - E \qquad [16]$$

On many undisturbed soil-mantled slopes, it is likely that the soil thickness approaches steady state, and production is balanced by erosion. One of the early challenges to soil scientists was determining the rate of soil production, a process that only recently became measureable with the use of cosmogenic radionuclides (Heimsath et al., 1997).

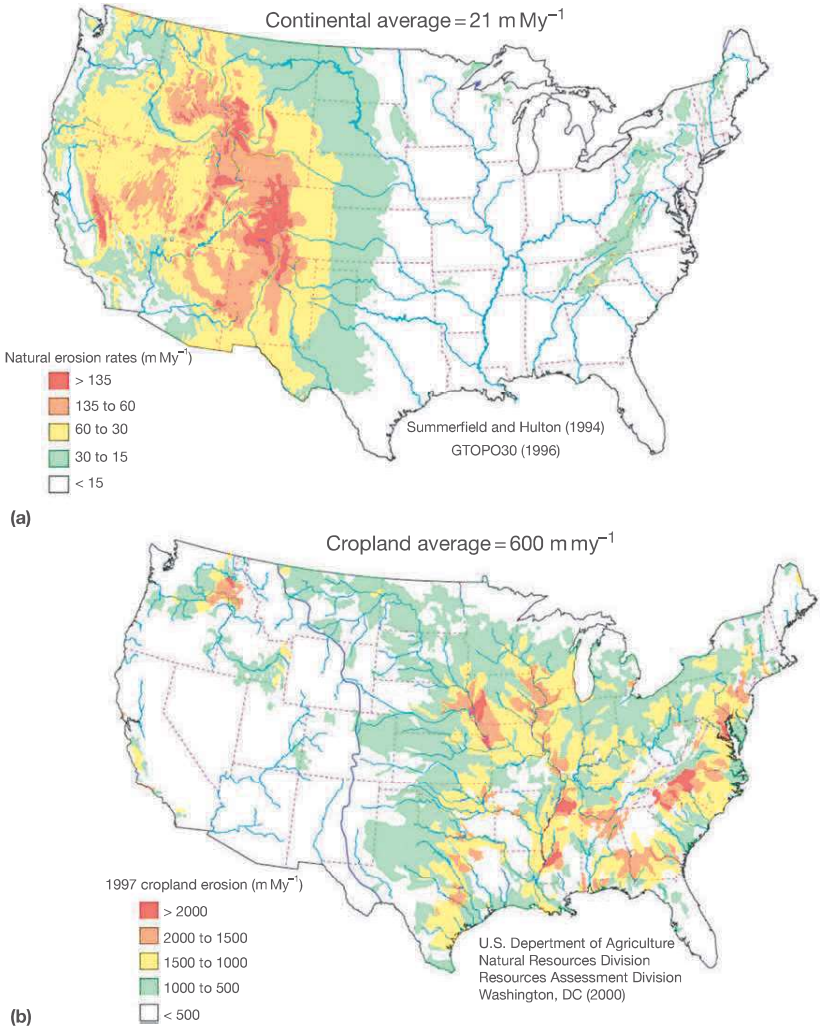

Figure 16 (a) The pre-European contact erosion rates and (b) 1997 erosion rates in the continental USA (reproduced from Wilkinson BH and McElroy BJ (2007) The impact of humans on continental erosion and sedimentation. *Geological Society of America Bulletin* 119: 140–156).

Recently, Montgomery (2007) reopened the discussion of soil sustainability under accelerated erosion using the model in eqn [16]. Under accelerated erosion, soil thickness is no longer steady state, the rate of soil thinning is thus $E-P$, and the time to completely strip the soil mantle is:

$$T = H/(E-P) \qquad [17]$$

If soil sustainability is defined as maintaining a steady soil thickness, the data in **Figure 13** suggest that the maximum rates of erosion can only be between 50 and 100 m My. This is much less than that which actually occurs (**Figure 16**) or the USDA recommended rate of ~400–1000 m My^{-1} (Schertz, 1983) based on poorly constrained data obtained before the advent of recent quantitative geomorphic and pedogenic methods.

What do the current erosion rates mean in terms of soil formation and geochemistry? If a soil mantle of 50 cm could be somehow maintained under a plausible agricultural erosion rate of 1 m ky (1000 m My), then the residence time would be 500 years. One fundamental attribute of soils in humid regions is the presence of an A horizon, representing the net accumulation of organic C and N from atmospheric sources. The mass balance of both can be described by an input/output model:

$$\frac{dC}{dt} = I - k_m C \qquad [18]$$

where C = concentration of either organic C or N, I = inputs (which differ for C and N), and k_m = a microbial degradation rate constant. If integrated for the boundary condition of no C or N at $t = 0$, the result is:

$$C_t = \frac{1}{k}\left(I - Ie^{-k_m t}\right) \qquad [19]$$

The decomposition constant, reflecting the metabolic rate that microbes decompose organic matter, is strongly dependent on climate (Amundson, 2001; Trumbore et al., 1996). On rapidly eroding soils, Stallard (1998) recognized that erosion is a significant means of C removal, and as such represents an additional loss that can be formalized with the addition of another rate constant, k_e:

$$C_t = \frac{1}{k_e + k_m}\left(I - Ie^{-(k_m+k_e)t}\right) \quad [20]$$

Since at steady state, total $C = I/k$, the steady state pool under rapidly eroding conditions will understandably be smaller than that of soils affected only by creep. However, Stallard (1998) recognized that if the eroded C is quickly buried and stabilized (in wet, low O_2 environments), the continuous erosive removal (and burial) of C would represent an ongoing sink of atmospheric CO_2. When scaled up to a global level, the possible C sink is on the order of 0.5–1.0 Gt C year^{-1}. The hypothesis of Stallard has recently been reevaluated by van Oost et al. (2007). Using revised estimates of global soil erosion, and a slightly lower projected rate of soil C rejuvenation in response to erosion, they estimated a global C sink of 0.06–0.27 Gt C year^{-1} – still a significant C flux (**Figure 17**).

While accelerated erosion appears to possibly have an unanticipated positive impact on the global C cycle by serving as an ongoing sink for atmospheric CO_2, the global combined impacts on other elemental cycles are less positive. First, the removal of A horizons in turn removes the important nutrients N and P. Quinton et al. (2010) estimate that the annual lateral transport of these elements by erosion in many regions nearly match the quantities added each year as fertilizer. Fertilizer N is largely produced by the conversion of atmospheric N_2 to NH_3 using natural gas as an energy source. About 1% of the annual global fossil fuel budget is presently used for N fertilizer production (Smil, 2004), and the cost of this will surely rise as oil and gas production soon pass their peak rates. Phosphorus is a rock-derived element. Global reserves are limited and transport is required. It has been suggested that the planet is presently nearing peak P (Childers et al., 2011), and that cost and availability of this resource will become major issues in the near future.

As natural erosion rates increase, the chemical weathering rates have been observed to increase in many locations (Riebe et al., 2004). Maher (2010) has suggested, based on the modeling scenarios, that this is largely driven by the fact that rapid erosion leaves behind soil minerals far from chemical equilibrium, thus promoting more rapid weathering the more rapidly soil erodes (eqns [5] and [6]). The impact of accelerated erosion on chemical weathering is much less understood. Given the weathering front advances even in tropical environment (**Figure 13**) are less than erosion rates in many agricultural settings, it seems plausible that mineral weathering rates should approach maximum rates observed in the laboratory under conditions of high accelerated erosion rates.

7.1.5.1 Accelerated Soil Formation Under Agriculture

Nearly 90% of global fresh water use is for agriculture (Scanlon et al., 2007; **Figure 18**). Since irrigation is applied in regions with an overall rainfall deficit (arid to semiarid climates), the addition of up to 0.75 m of additional water per year (along with fertilizers and amendments) causes an abrupt and profound change in the boundary conditions for soil formation.

Agricultural practices vary enormously with region and crop. **Table 2** compares the soil-forming conditions for uncultivated and cultivated land in the vicinity of the Merced River. Viewed differently, it is the equivalent of changing the climate of the region from its presently highly seasonal, semiarid condition to a climate and biotic system more reminiscent of the humid subtropics – with the additional effect of being first bulldozed. Given that chemical weathering rates should be approximately linearly proportional to fluid velocity (Maher, 2010), this change should at least impart an order of magnitude increase in chemical weathering rates of primary and secondary minerals. Somewhat surprisingly, extensive literature searching for this chapter revealed no study that made a comparative analysis of in situ weathering rates in natural and irrigated conditions. Thus, I review how other soil chemical properties (as opposed to pore water chemistry and short-term weathering rates) respond to land use change.

Amundson et al. (2003a) examined the combined agricultural and urban impacts on soil distribution and abundance in the USA. The goal of the study was to determine what fraction of the different soil series (the most-detailed level of soil

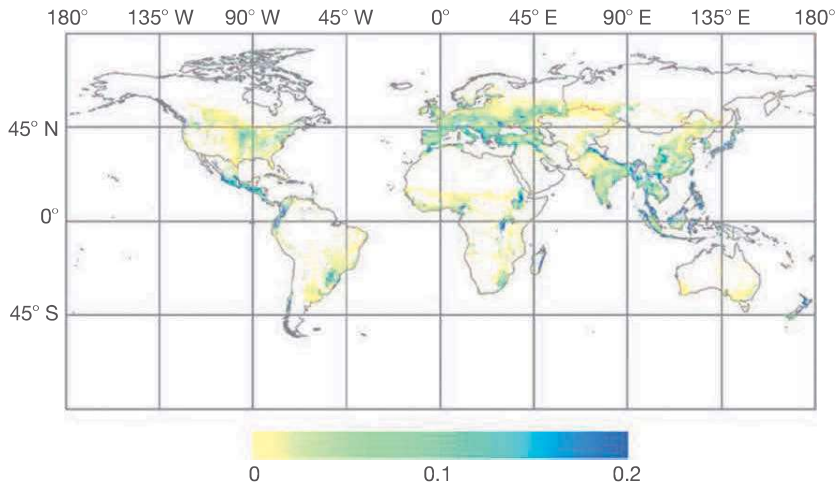

Figure 17 Global modeled rates of soil organic C erosion by tillage and water (reproduced from Van Oost K, Quine TA, Govers G, et al. (2007). The impact of agricultural soil erosion on the global carbon cycle. *Science* 318: 626–629). Units are in Mg C ha^{-1} year^{-1}.

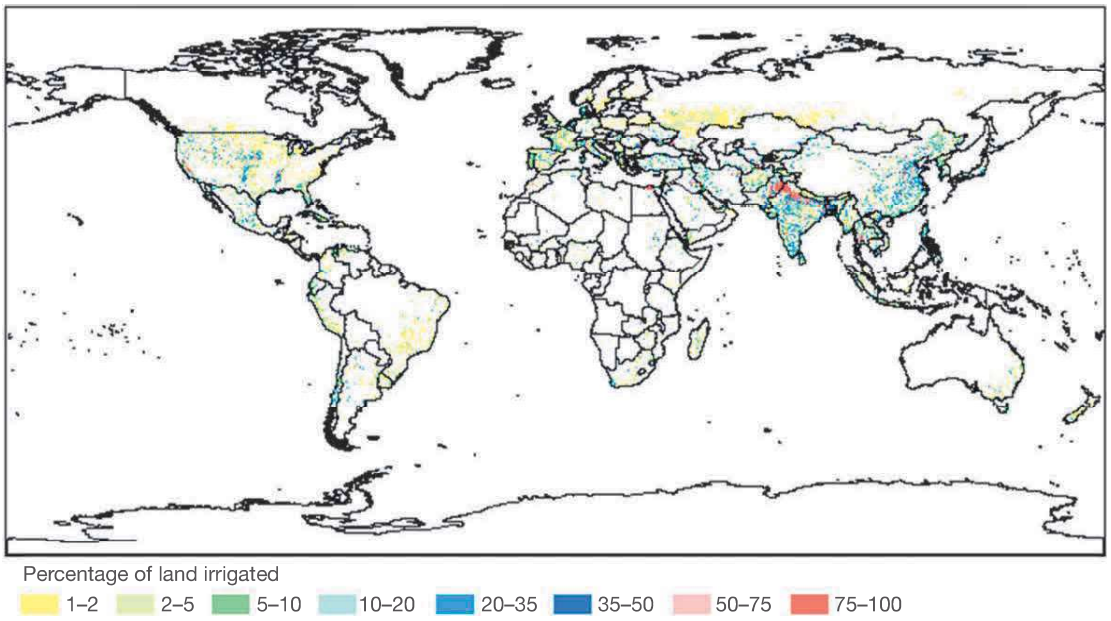

Figure 18 Map of the global distribution of irrigation. From http://www.fao.org/nr/water/aquastat/quickWMS/irrimap.htm.

Table 2 A comparison of the soil-forming boundary conditions for natural and irrigated soils in the eastern San Joaquin Valley of California

Property	*Natural*	*Irrigated*
MAP/irrigation (mm)	310	1000
Average soil temperature at 50 cm (°C)	16	~11–12
Biota	Annual grasses, forbs	Fruit and nut orchards, vineyards, alfalfa, cotton, tomatoes
Net primary production (kg $ha^{-1}year$)	1000–2000	15000 (alfalfa)
N addition (kg $ha^{-1}year^{-1}$)	10	200–300
S addition (kg $ha^{-1}year^{-1}$)	<3	3000–30000 (frequency variable)

A range of management types are included for the irrigated soil to provide a perspective of possible changes.

classification and the basis for soil mapping units) in the USA had been converted to agriculture or urban uses. To perform the calculation, a landuse map of the USA (the USGS Landsat classification) was overlain digitally on the soil basemap. Soils converted to agriculture or urban use experience an array of direct or indirect changes, but some of the key changes include tillage, irrigation, changes in biota, addition of acids or bases. For the purposes of their analyses, all these converted or managed soils were referred to as 'domesticated soils' – in a manner analogous to the changes in biological species (e.g., dogs, chickens) that occur under domestication. Soil series that had lost 50% or more of their area to combined human land uses were classified as 'endangered soils' (**Figure 19**). This map illustrates three points: (1) the potential magnitude of the human footprint on soil processes in many parts of the world, (2) the need to both preserve remaining undisturbed landscapes as reference points, and (3) the need to launch research to examine the soil formation processes systematically within this vast region of profoundly changed conditions.

Given this perspective, it is remarkable that there are no soil weathering studies on irrigated landscapes comparable to those of White et al. (1996, 2006) for undisturbed soils. The only two studies that appear to be available in California are the early studies of Amundson and Lund (1985) and Amundson and Smith (1988), who examined very select properties in a comparative analysis of natural and irrigated soils on the granitic alluvium in the eastern San Joaquin Valley, and alluvium derived from sedimentary rocks in the western San Joaquin Valley.

To contrast the environmental conditions between pre- and post-irrigation, Amundson and Smith (1988) monitored soil temperature, moisture, and CO_2 respiration in a natural young (<1 ky) soil in the arid western San Joaquin Valley relative to an adjacent site that had been converted to an almond orchard. **Figure 20(a)** shows that the average soil water contents were much higher in the irrigated site, and soil temperatures were cooler (due to both evaporation and shading of the surface), and that biological production of CO_2 (**Figure 20(b)**) was overall much higher, but was entirely asynchronous with the cycle in the natural soil. In the eastern San Joaquin Valley, Amundson and Lund (1985) focused on the rate and extent of irrigation water removal of salt from a naturally saline soil located near the terminal end of alluvial fans adjacent to the basin of the San Joaquin Valley. They found large and rapid (<10 years) removal of salts from the upper 1 m of the profiles (~75000 kg ha^{-1}). Based on the x-ray diffraction analyses of the clay fraction, they also found some evidence for the relative

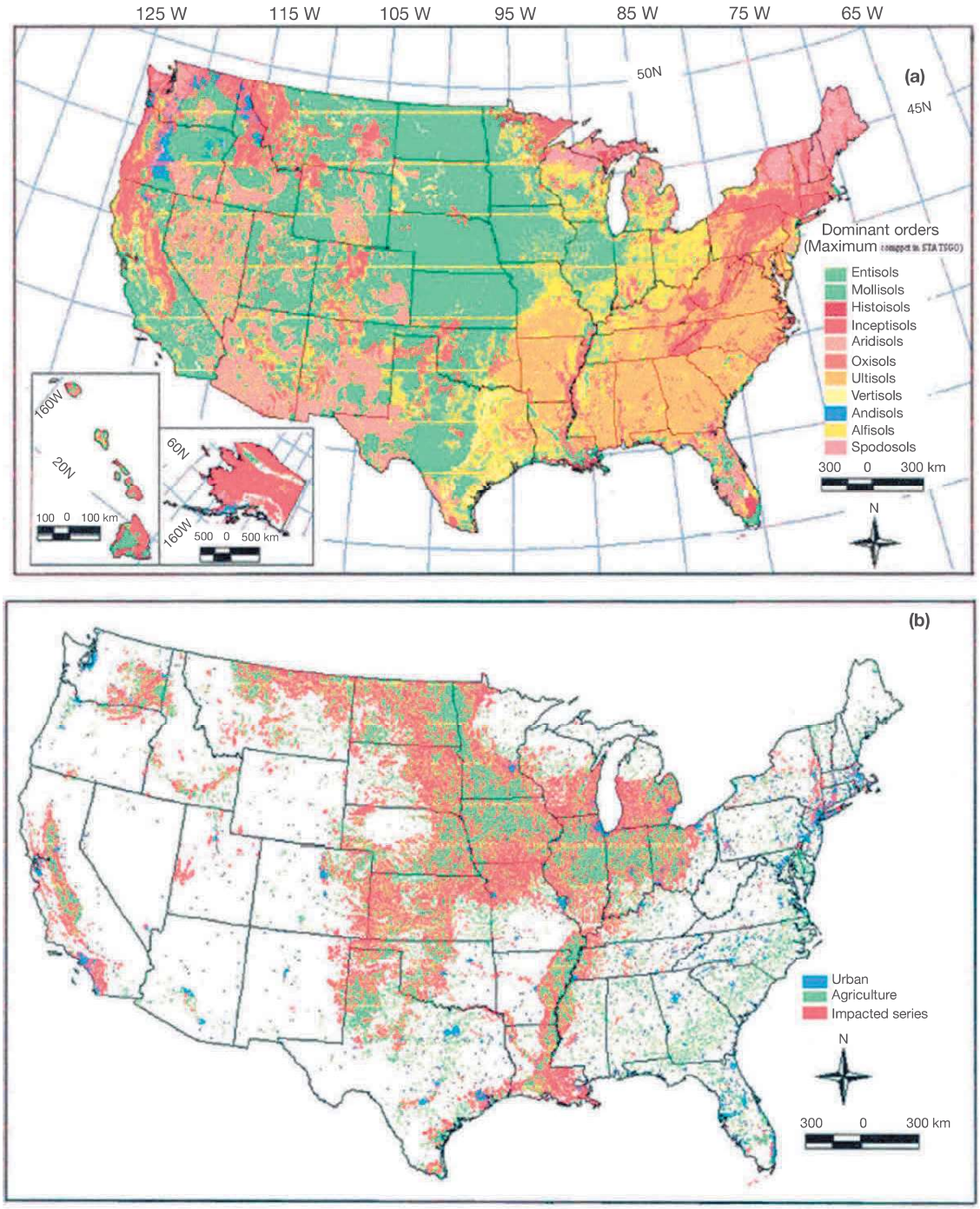

Figure 19 (a) The natural distribution of soil orders in the USA and (b) the distribution of soil series that have 50% or more of their area in agricultural or urban use (impacted series). Also shown in (b) is the area of agriculture and urban land in the USA.

loss of smectite, and some gain of kaolinite, after >25 years of intensive irrigation and farming.

Within the past decade, the NRCS has begun to focus more attention on human impacted soils in California and elsewhere, mapping highly disturbed soils as new series in the *Arent* category of the US Soil Taxonomy (Ar=L. arare, to plow; Ent='recent'). In some cases, highly detailed chemical and physical data for both the 'Arent' and its natural counterpart are available on the NRCS database. Presently, there are 36 Arents mapped in the USA and 5 in California. To illustrate the magnitude of chemical and physical change, here I compare a soil formed on the toe of alluvial fans derived from latest Pleistocene/earliest Holocene outwash from the adjacent grantic Sierra Nevada. The evaporative enrichment of salts

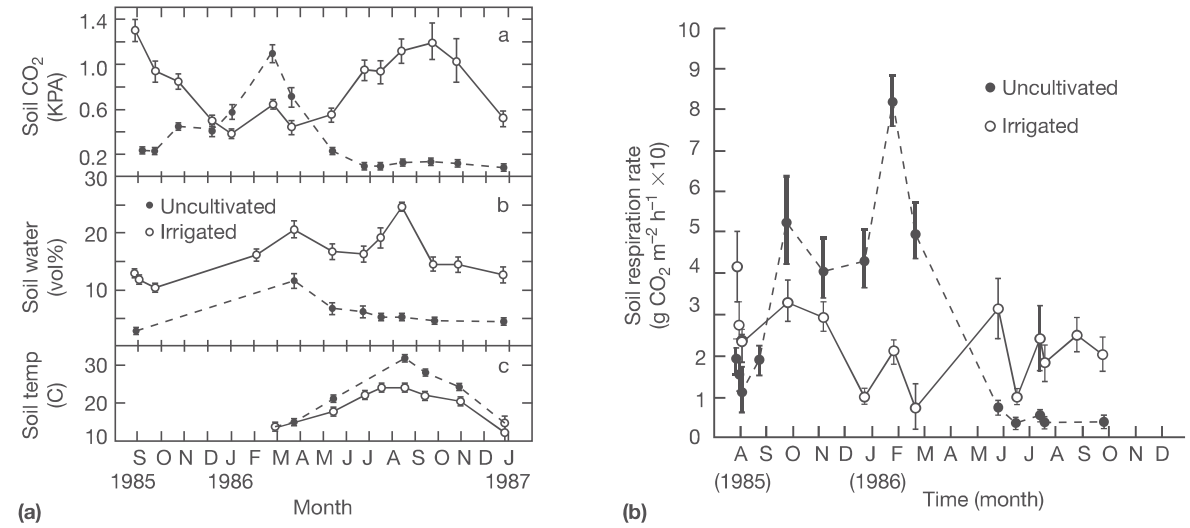

Figure 20 (a) Variations in average soil conditions and (b) soil CO_2 respiration rates for adjacent native and irrigated soils in the San Joaquin Valley of California. Reproduced from Amundson RG and Smith VS (1988) Annual cycles of physical and biological properties in an uncultivated and irrigated soil in the San Joaquin Valley of California. *Agriculture, Ecosystems and Environment* 20: 195–208.

from shallow groundwater creates high pH environments that promote rapid silicate weathering, secondary clay formation (**Figure 21(a)**) (including the unusual (for soils) zeolite analcime (**Figure 21(d)**)), an opaline Si-cemented hard pan, carbonates, high Na and pH (**Figure 21(c)**), and high soluble salt concentrations – as indicated by electrical conductivity (**Figure 21(b)**).

Conversion of these soils to agriculture involves deep ripping (**Figure 22**), application of gypsum and elemental S (to lower pH and remove Na), and the application of excess irrigation water. The result of these combined processes is a physical mixing of the soil and the disruption of the clay-rich Bt horizon (**Figure 21(a)**), the stripping of total soluble salts (**Figure 21(b)**), reduction in pH (**Figure 21(c)**), and apparent declines in the relative abundance of montmorillinite (**Figure 21(e)**) and analcime (**Figure 21(d)**) in the $<2\,\mu m$ fraction of the soil. The organic C profiles have similar shapes (though the surface content of the undisturbed site is higher (**Figure 21(f)**)). The total C in the undisturbed profile is 2.6 kg m^{-2}, while than in the irrigated soil is 3.6 kg m^{-2}. The apparent increase in C is consistent with higher C inputs into the soil and reductions in soil temperature. Since the average global soil C storage is about 10 kg m^{-2}, both soils are very low in organic matter, as expected for arid climates (Amundson, 2001).

Rivers draining agricultural areas should integrate the weathering products from these landscapes. However, as Raymond and Cole (2003) point out, it has proven difficult to tease the agricultural imprint from the baseline processes in river chemistry data. In their paper, however, the authors were able show that over a 48-year period, there has been an increase in the concentration of bicarbonate in the Mississippi River, one consistent with agricultural land use. The authors speculated due to the enormous agricultural footprint, pre-agricultural alkalinity export form the Mississippi may have been one half to one third of the present fluxes.

The human transformation of landscapes is a major global force, and one which from a geochemical perspective (except for the soil C and N cycles, which were only briefly examined here) is largely unknown.

7.1.6 Soil Geochemistry in Deserts

In the past decade, we have learned much about the geochemistry of hyperarid deserts on Earth: the warm, very dry Atacama Desert of Chile and the cold, dry Dry Valleys of Antarctica. In the soils of these regions, the driving geochemical processes are abiotic, and chemical weathering of silicates is nearly negligible (Ewing et al., 2006). These are regions where soil geochemistry is dominated by the slow accumulation of atmospheric solutes and their partial vertical separation and transport by occasional inputs of meteoric waters. As a result of this ongoing research, we now know much more about the behavior of carbonates, sulfates, and chlorides in deserts – particularly from stable isotope studies of these minerals.

One of the key revelations of isotope research in arid and hyperarid soils on Earth is that *stable isotopes in soils are rarely conservative tracers of element source*, and instead reflect complex postdepositional processes caused by aqueous or gaseous transport. Below, I briefly discuss some general aspects of the behavior of major salts in arid and hyperarid soils, particularly their isotopic composition.

Calcite is nearly ubiquitous in arid soils, with the Ca commonly derived largely from dust and aerosols, the C from soil CO_2, and the O from soil water. Due to root respiration and decomposition of organic matter, soils on Earth have CO_2 concentrations orders of magnitude higher than the overlying atmosphere, and this CO_2 is transported to the atmosphere via molecular diffusion. Cerling (1984), in a seminal paper, showed that a soil CO_2 model incorporating in soil production and diffusion to the atmosphere replicated both measured soil

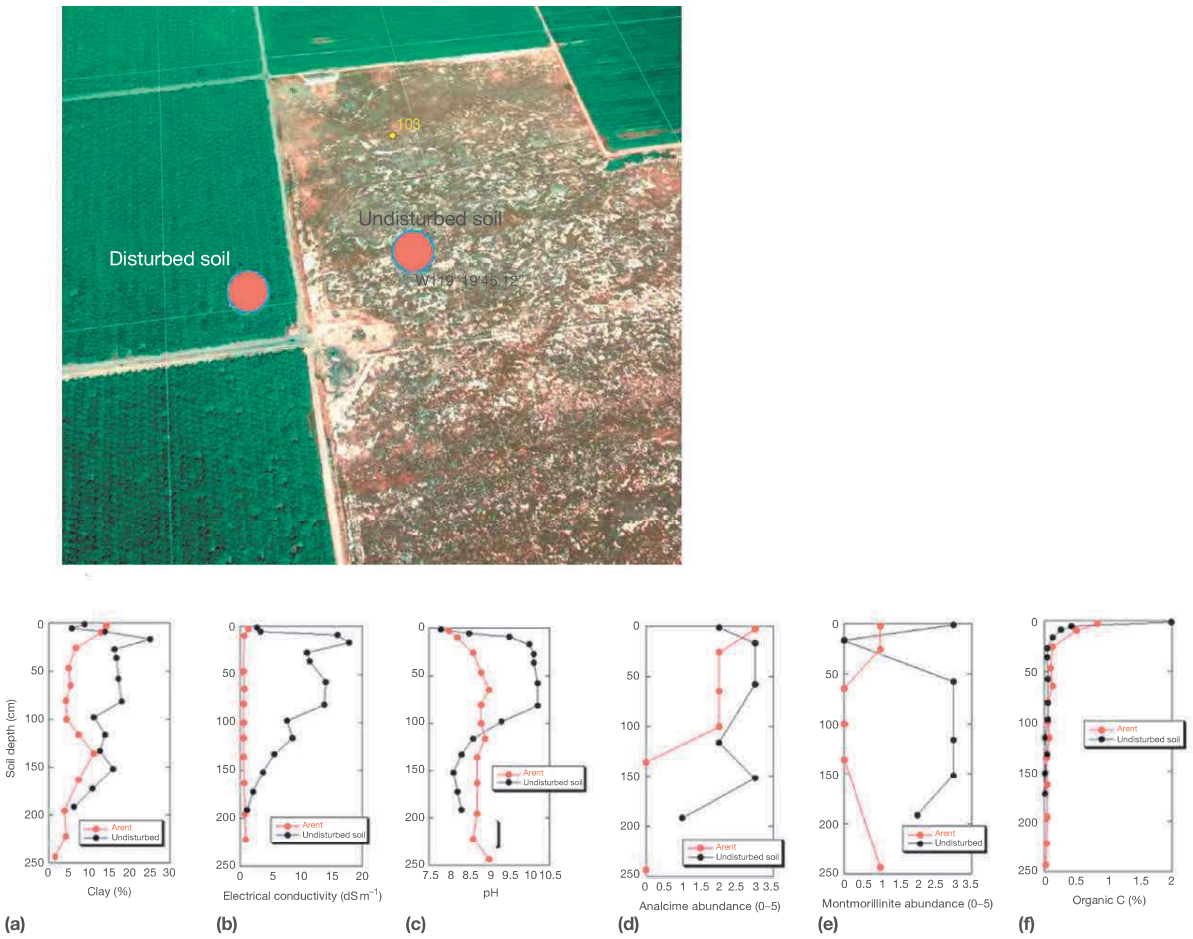

Figure 21 The upper panel is a Google Earth image (located to N) showing the location of the undisturbed soil (Jerryslu) and the paired cultivated soil (Atesh) that has been converted to an Arent. The lower diagrams show comparisons of (a) clay, (b) electrical conductivity (measure of soluble salts), (c) pH, (d) analclime abundance (0 = not report, 5 = very abundant), (e) montmorillinite, and (f) organic C versus depth.

CO_2 C isotope profiles and any carbonate that formed in the soil. In this model, the C isotope composition of carbonate is a function of the rate and isotope composition of the biological source of the CO_2, the concentration and isotopic composition of the atmosphere, and soil depth (plus an equilibrium fractionation factor):

$$R_s^{13} = \frac{\frac{\phi R_p^{13}}{D_s^{13}}\left(Lz - \frac{z^2}{2}\right) + C_{atm}R_{atm}^{13}}{\frac{\phi}{D_s}\left(Lz - \frac{z^2}{2}\right) + C_{atm}} \qquad [21]$$

where $R = {}^{13}C/{}^{12}C$ ratio of soil CO_2 (s) (or any carbonate that forms from it at equilibrium), biological production (p), or the atmosphere (atm); D = diffusion coefficient of regular CO_2 or ${}^{13}CO_2$; L = depth of the base of soil; C_{atm} = concentration of CO_2 in the atmosphere; and z = depth.

Figure 23 shows the C isotope depth profile of carbonate in a very arid Mojave Desert soils (from Wang et al., 1996). The graph shows that the C isotope composition of the soil carbonate varies by about 8‰ over only 80 cm of soil depth and that the depth profile can be matched by eqn [21] using the appropriate parameters for the site. Recognizing that these patterns occur is critical for sampling and interpreting isotopic analyses of paleosols, for example. As eqn [21] indicates, the C isotope ratio of soil CO_2, and any carbonate that forms in equilibrium with it, reflects both the C isotope ratio of plant respiration (and the mix of C3 versus C4 plants) and the concentration of atm CO_2. Thus, beginning with Cerling's (1984) and Quade et al.'s (1989) work, paleosols have been important archives for paleovegetation and paleo-CO_2 studies. However, the C isotope analyses of single sample, from a poorly defined location, cannot be interpreted unambiguously, and there is a greater need in paleopedology research for depth-dependent sampling of paleosols.

Sulfate is ubiquitous in hyperarid soils on Earth. Stable S and O isotope analyses of sulfate in soils have become methodologically convenient in roughly the past decade. The first major study of isotopes in Atacama soil sulfate (Rech et al. 2003) was based on the assumption that sulfate in the upper portion of the soil along a gradient from the coast to the Andes would reveal differences in the source of the sulfate (marine vs. terrestrial). However, Ewing et al. (2008) discovered that the range of values in a depth profile of S and O isotopes in *a single soil* equaled or exceeded the isotope variation in all the surface samples in the entire desert (in a 150 cm soil profile,

the S and O isotopes covaried by more than 10‰). Ewing et al. (2008) found that depth profiles of S, O, and Ca isotopes in the sulfate were all explainable using a Rayleigh-type model, where $CaSO_4$ is added at the soil surface, then is dissolved and moved downward with rain, and then reprecipitated at greater depths:

$$\delta_{\text{solid}}(z) = \left(\delta_{\text{inputs}}(z) + 1000\right) f^{\alpha_{\text{w-s}}-1} - 1000 \qquad [22]$$

where δ_{solid} = the δ value for the solid at depth z, where δ_{inputs} = the δ value of the dissolved inputs (from above) at depth z, $\alpha_{\text{w-s}}$ = the sulfate aqueous to solid isotope fractionation factor, and f = the fraction of the total sulfate inventory at depth z relative to the total inventory from z to the base of the soil. The δ_{input} value and depth z can be calculated from the following relation:

$$\delta_{\text{input}}(z+1) = \frac{\left[\delta_{\text{input}}(z)\text{SO}_{4\,\text{inputs}}(z) - \delta_{\text{solid}}(z)\text{SO}_{4\,\text{solid}}(z)\right]}{\text{SO}_4(z)} \qquad [23]$$

We have demonstrated that this model explains sulfate isotope profiles in Chile as well as much of the depth variation of sulfate in the soils of the Dry Valleys of Antarctica (Amundson et al., 2012). **Figure 24** shows the measured and modeled S and Ca isotope profile in sulfate in a Pliocene-aged Atacama Desert soil (Ewing et al., 2008). S isotopes have about a 10‰ variation, while the Ca isotopes have about a 2.5‰ variation: about 1/2 of the observed Ca isotope variability on Earth (DePaolo, 2004). For both elements, eqns [22] and [23] provide strong fits with observations, indicating physical processes are driving the fractionation. Additionally, the isotope values at most depths bear little relation to the value of the atmospheric source.

Nitrate is concentrated, along with halite, in hyperarid soils of Chile (Ewing et al., 2007; Michalski et al., 2004) and Antarctica (Michalski et al., 2005). The global distribution of soil N and N isotopes in Earth soils varies greatly, and systematically, with climate (Amundson et al., 2003b). Briefly, climatic conditions that favor the loss of isotopically depleted N forms (aqueous NO_3^- or gaseous N_2O or N_2) cause the remaining soil N to become enriched in ^{15}N, and generally the

Figure 22 (a) A 'slip plow' deeply ripping a field and (b) an excavation showing the physical disruption caused by the tillage, and the disruption of the natural soil layers (reproduced from Eddy D (2008) Prepare for soil take-off in walnut orchards. Growing Produce. com.).

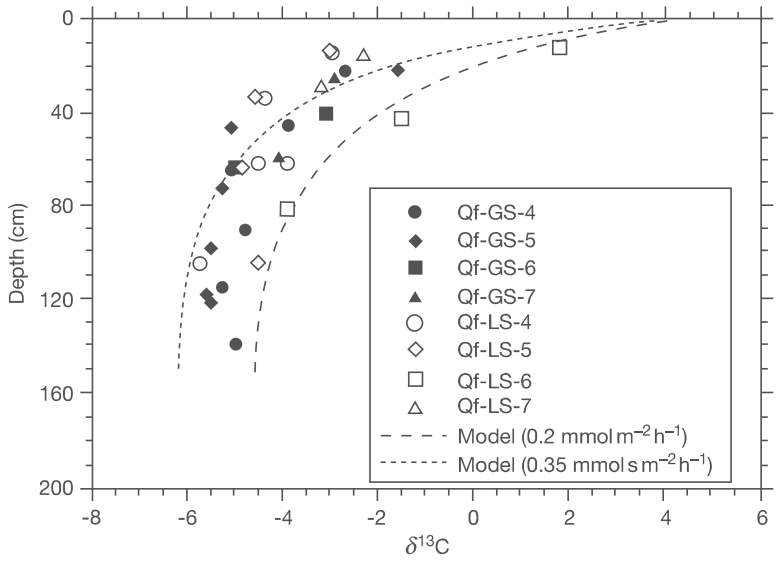

Figure 23 Measured (points) and modeled (line) soil carbonate C isotope values for soils located in the Mojave Desert, NV. Reproduced from Wang Y, McDonald E, Amundson R, McFadden L, and Chadwick O (1996) An isotopic study of soils in chronological sequences of alluvial deposits, Providence Mountains, California. *Geological Society of America Bulletin* 108: 379–391.

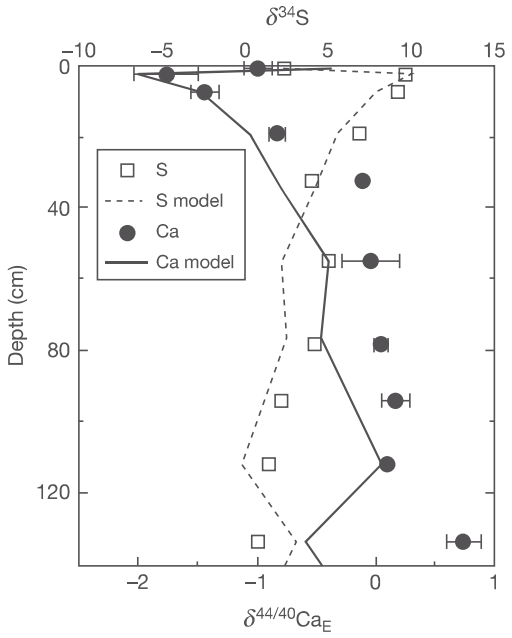

Figure 24 Ca and S isotope values observed (symbols) and modeled (lines) using a Rayleigh model. Input values were total isotopic values for the soil inventory (δ^{34}S = 1.98‰ and δ^{44}Ca = −0.37‰). Fractionation factors were from the literature (Ewing et al., 2008).

^{15}N content of soils increases with increasing aridity. However, we have also shown that there is a fundamental threshold in this relationship at the biotic/abiotic boundary on Earth (Ewing et al., 2007). Once the biotic/abiotic threshold is crossed (due to loss of water), microbial reduction of soil N forms to N_2 ceases, and soil becomes a repository for N. In the Atacama Desert, Ewing et al. (2007) showed that as rainfall declines, the soil N pool shifts from an organic driven pool to one dominated entirely by inorganic forms, particularly sodium nitrate. Also, they found (using triple O isotope analyses) that about 80% of the considerable NO_3^- in the driest soils is atmospheric N (formed in troposphere with ozone and unaltered by soil biology), but that there was nearly a 10‰ variation in N isotopes with soil depth (Ewing et al., 2007). These complex N isotope depth trends likely reflect the impact of very modest, but fractionating, biological losses of N during rare rainfall events. Also, and some abiotic fractionation may occur during downward migration. As of now, there appears to be no work on isotopic fractionation between NO_3^- and solid $NaNO_3$.

Hyperarid soils offer an entirely different set of chemical processes relative to the remainder of the more humid, and more biotic, Earth. However, they share more in common with the presently dry and cold planet Mars, and the surprising things we have learned about this planet in the past decade.

7.1.7 Soil Formation on Mars

Soil formation as we know it in humid regions on Earth involves the alteration of Si-rich rock and minerals by aqueous solutions. The only other known planet where this has occurred or is occurring is Mars. Since the last version of this chapter, rovers have been exploring the surface chemistry and mineralogy of Mars continuously: Spirit (3 January 2004–22 March 2010), Opportunity (24 January 2004–present (October, 2011)), and Pheonix (25 May 2008–2 November 2008). These missions, along with those of Viking and Pathfinder, are providing a wealth of chemical, mineralogical, and visual pedological information about the Martian surface. Here, for brevity, I focus on soil formation information at Gusev Crater (Spirit), Meridiani Planum (Opportunity), and the northern polar region (Phoenix), to illustrate the diversity of processes that formed Martian soil, and the relative diversity of soil types.

Gusev Crater is a large impact basin that is believed to have been overlain by basalt flows (McGlynn et al., 2011). Both Spirit and Opportunity were equipped with alpha particle x-ray spectrometers capable of measuring major rock-forming elements (Gellert et al., 2004). The mobile arm that could be directed toward soil and rock targets was also equipped with a rotating brush and abrasive drill to remove surface dust or debris. Finally, both rovers were capable of 'excavating' shallow soil exposures of 10–15 cm by rotating one of their wheels, thereby making shallow geochemical profiles possible (**Figure 25(a)**). Because the Spirit rover at Gusev Crater was able to conveniently examine the elemental chemistry of both rocks (scattered over the land surface) and shallow soil profiles, it is possible to calculate elemental gains and losses of elements in the soils using the approach outlined in eqn [3]. The surprising result of this comparison is that the soils show considerable losses of Si and other key rock-forming elements (along with gains of S and Cl salts) relative to the pristine basalt (the exterior of the basalt itself shows considerable accumulations of dust as well as aqueous alteration (Christiansen et al., 2004; Gellert et al., 2006; **Figure 25(b)**)). The apparent chemical depletions of Si, Al, etc., are also evident in wheel-excavations, indicating that the depletions were not just reflective of a surficial eolian dust coating. Amundson et al. (2008) proposed that these patterns are suggestive of in situ chemical weathering and downward migration of weathering products by aqueous transport. However, given the shallow nature of the excavations, this hypothesis could not be fully tested. The apparent gains of S and Cl in the soil surface (and corresponding cations) had been observed in earlier missions and are considered to be the result of atmospheric deposition (Clark et al., 1982). Given that the accumulation of water-soluble salts is incompatible with weathering and losses of Si, it was proposed that this represented a later (or present) stage of salt accumulation over earlier weathered material.

Turning to Earth, Amundson et al. (2008) used published soil geochemical data along a rainfall gradient from some of the wettest (Hawaii) to driest (Atacama Desert) regions on earth, looking for the geochemical fingerprint of rainfall on the upper 20 cm, a depth roughly equivalent to a rover observation. The sites in each climate zone ranged from 10^5 to 10^6 years, roughly the longest duration of weathering usually possible on the tectonically and climatically active Earth. This fingerprint (**Figure 25(c)**) showed that on Earth, significant moisture is required to deplete the surface in a manner similar to that at Gusev Crater. Secondly, the authors also noted that ancient soils on earth (known as *relict soils*) commonly are exposed to multiple climate conditions and can retain evidence

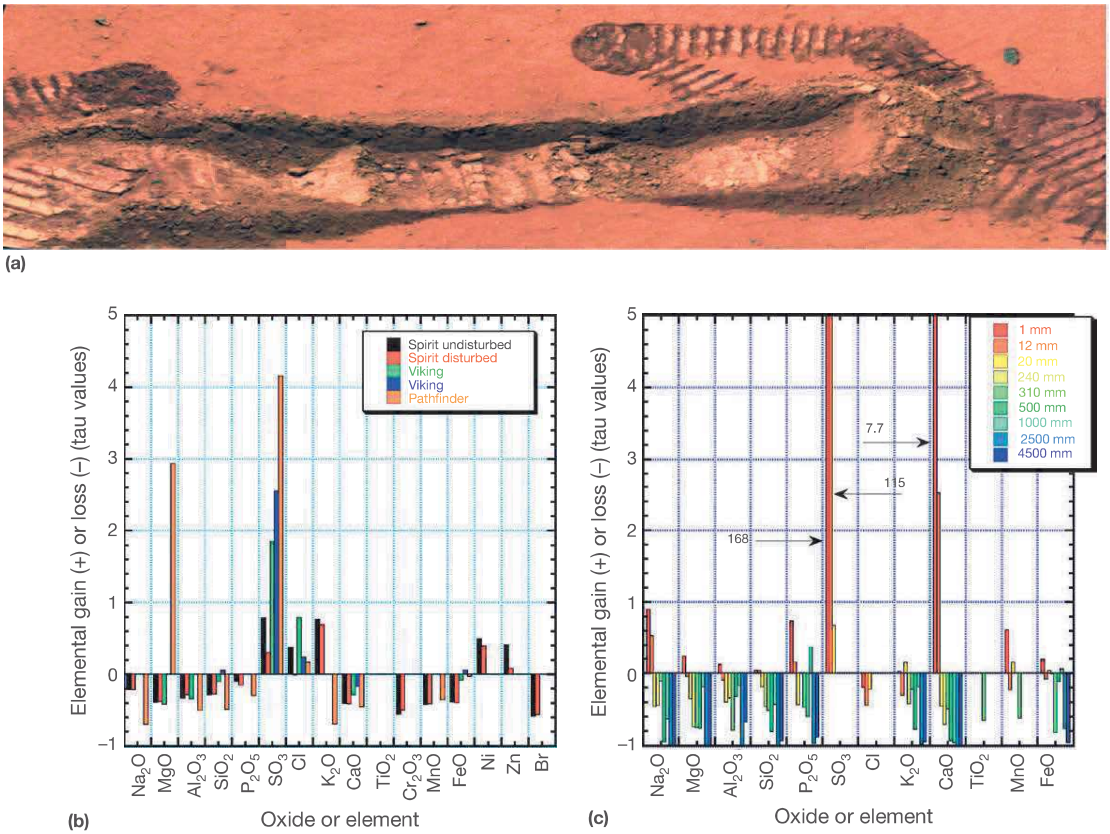

Figure 25 (a) Image of Spirit Rover wheel 'excavations' at Gusev Crater (Wang et al., 2006), (b) tau values of Spirit and Pathfinder soils relative to local bedrock, and (c) the chemical fingerprint of rainfall on the upper 20 cm of soil on earth ((b and c) reproduced from Amundson R, Ewing S, Dietrich W, et al. (2008) On the *in situ* aqueous alteration of soils on Mars. *Geochimica et Cosmochimica Acta* 72: 3845–3864).

of past climate conditions, particularly if the shift is from more humid to arid conditions. Thus, the soils at Gusev could be interpreted as recording a long shift from semiarid to hyperarid climatic conditions over a prolonged episode of time.

The authors also noted that the salts in soils at Gusev Crater exhibit evidence of some near-surface chemical partitioning suggestive of very modest recent surficial penetration of moisture. This interpretation of late stage aqueous transport has also been proposed for a near-surface solute profile observed in the nearby Columbia Hills (Arvidson et al., 2010). At the final resting place of the spirit Rover, the presence of relatively insoluble minerals at the immediate surface, and the presence of a Fe-sulfate rich layer immediately below (that corresponds to the topography), is viewed as representing downward movement of "films of water associated with frost formation and snowpack development . . . during periods of high obliquity."

In contrast to the lithology of Gusev Crater, Meridiani Planum is a broad plain of wind-swept dust and hematite dunes that overlie a thick sedimentary sequence of wind and (possibly) water deposited sulfates and weathered basalt grains. Numerous meteorite impacts, coupled with minor postimpact diagenesis, have created approachable (from the rover's perspective) geological/pedological profiles more than 6 m deep. Two craters with exceptional exposures have been examined: Endurance (**Figure 26(a)**) and Victoria (**Figure 26(b)**). At the time of this writing, only preliminary geochemistry of the Victoria crater has been published (Arvidson et al., 2011). At Endurance, Amundson et al. (2008), using eqn [1] and a comparison to both fresh basalt and the base of the profile found little geochemical variation with depth in silicate-associated elements, but substantial variations with depth of S, Cl, and Br (**Figure 26(c)**). The S and Cl profiles shared similarities to those found in Pliocene-aged soils in the Atacama Desert of Chile (**Figure 26(d)**), where solubility differences between the anhydrite/gypsum and halite result in chemical partitioning with depth caused by downward migrating waters. While upward migration of fluids from a shallow groundwater has been proposed as a process impacting this locality (McLennan et al., 2005), the salt profiles are more consistent with the observed (Ewing et al., 2006) and modeled (Walvoord, 2002) results of downward migrating water.

Victoria Crater (**Figure 26(b)**) lies approximately 6 km from Endurance, and the rover Opportunity explored this crater in 2008. While the sedimentary rock shares many similarities to Endurance Crater, one notable addition is the presence of an ~1 m thick 'diagenesis zone' that was present prior to impact (the 'Smith' unit, **Figure 25(b)**), that is now covered by a mantle of ejecta. Whether this represents a soil weathering zone awaits the publication of the rover observations. However, a simple comparison of depth profiles (S and Cl vs. Si) for both profiles (Arvidson et al., 2011) reveals regional similarities in the near-surface solute profiles consistent with a very modest surficial input of water (**Figure 27(d)**).

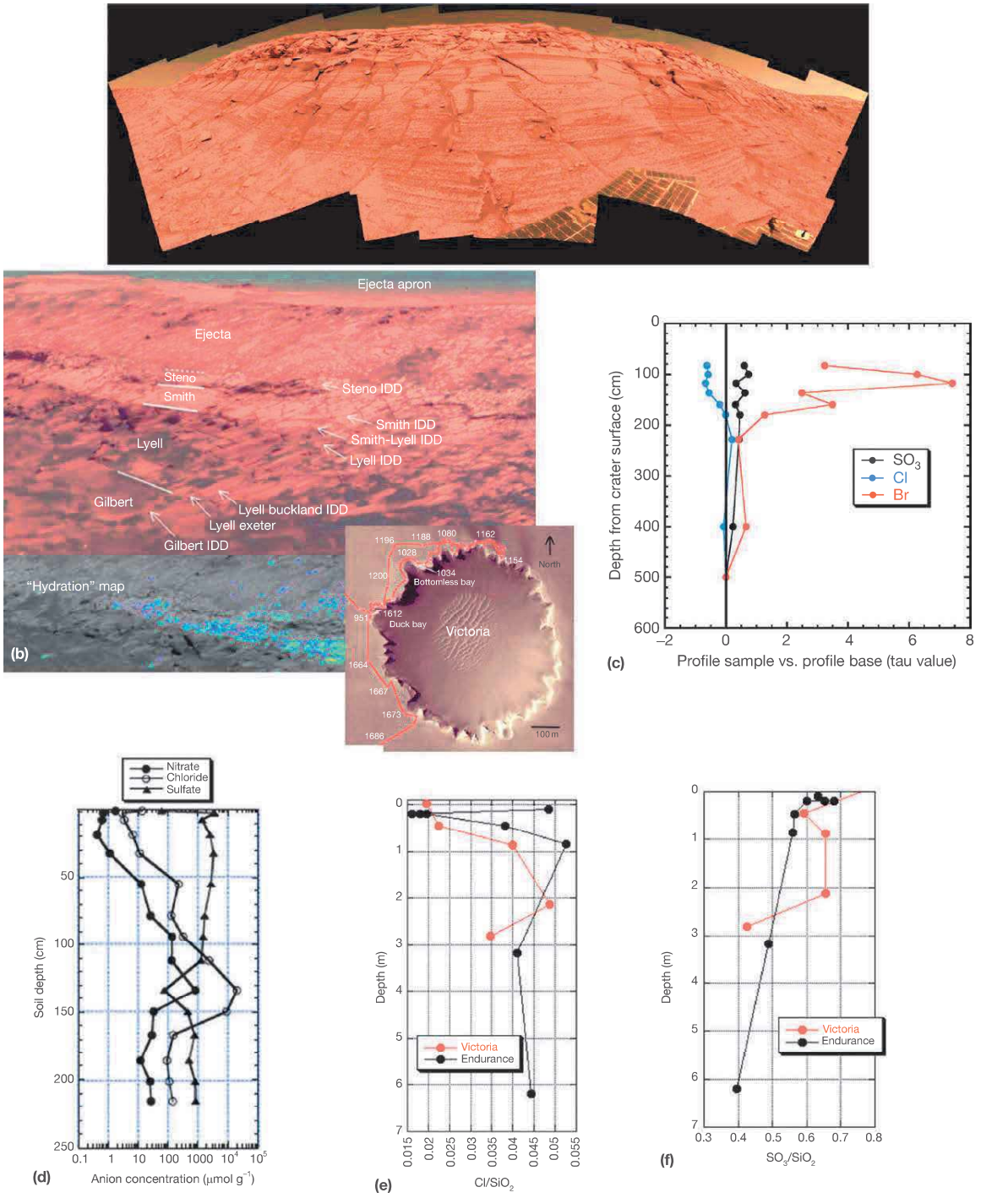

Figure 26 (a) Image of Endurance Crater, (b) Victoria Crater (Arvidson et al., 2011), (c) tau values of S, Cl, and Br at Endurance, (d) soil chemical profiles in a hyperarid soil in Chile (both (c and d) reproduced from Amundson R, Ewing S, Dietrich W, et al. (2008) On the in situ aqueous alteration of soils on Mars. *Geochimica et Cosmochimica Acta* 72: 3845–3864), (e) Cl/SiO_2 and (f) SO_3/SiO_2 profiles for both Endurance and Victoria craters (data from Arvidson et al., 2011).

The Phoenix lander, which explored the northern plains of Mars, represented a far different scientific payload and set of objectives than the rovers. One of the most distinctive pedogenic observations is the polygonal pattern of the landsurface (Mellon et al., 2009; **Figure 27(a)**, **27(b)**), one consistent with cryoturbation processes observed on Earth (Sletten et al., 2003; **Figure 27(c)**). Indeed, water ice was revealed during both landing and during excavations by the mechanical shovel aboard the lander (Cull et al., 2010a). Chemically, the presence of perchlorate and carbonate in the soils (below the

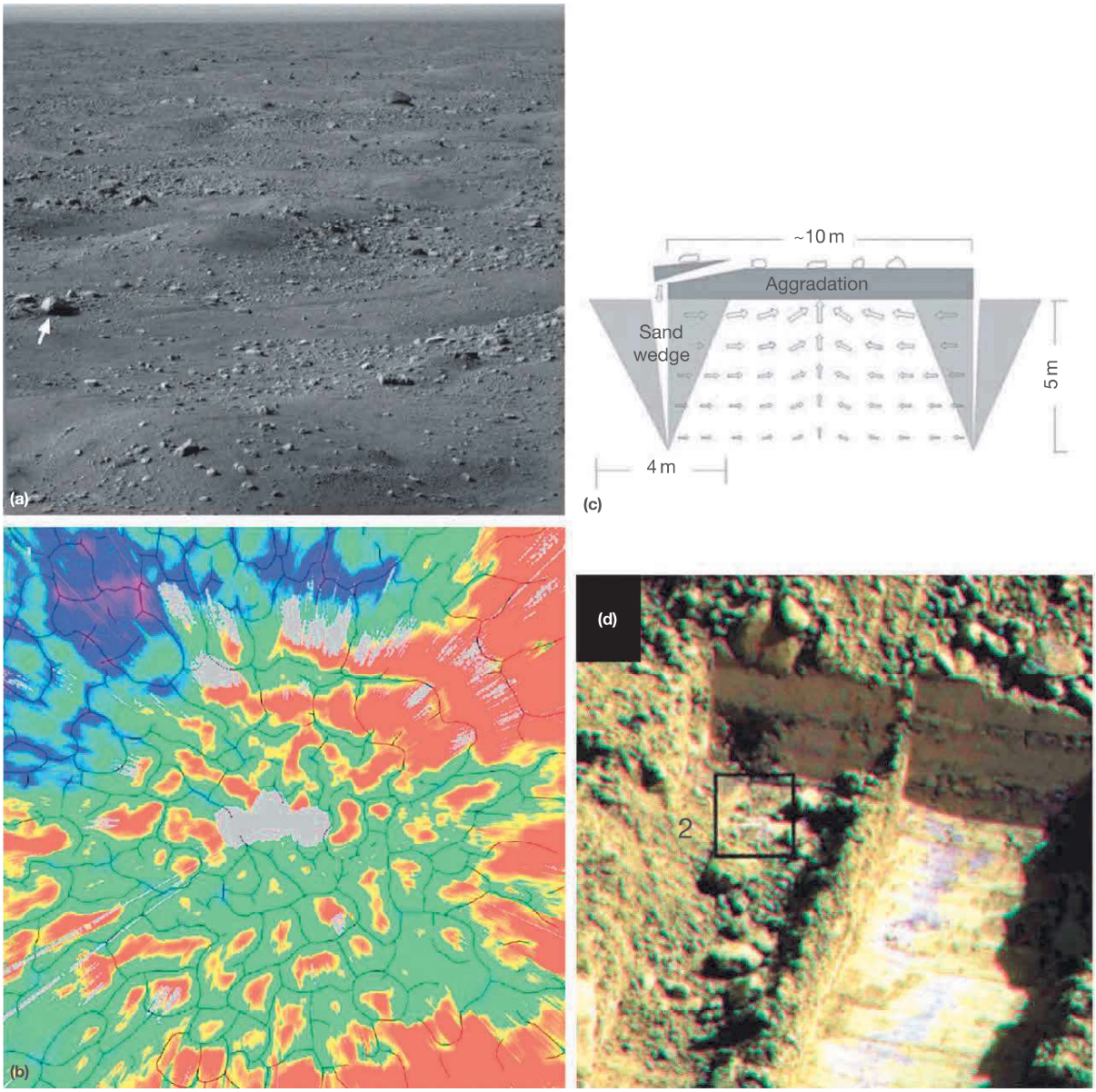

Figure 27 (a) Image of the microrelief surrounding the Phoenix lander, (b) a map of the patterned ground surrounding the lander (in center of image), with higher areas in red, and lowest areas in blue (50 × 50 m) (both (a and b) reproduced from Mellon MT, Malin MC, Arvidson RE, et al. (2009) The periglacial landscape at the Phoenix lander site. *Journal of Geophysical Research - Planets* 114: EOOEO6, http://dx.doi.org/10.1029/2009JE003418), (c) a schematic illustrating the formation of patterned ground in Antarctica, with the formation of cracks that fill with sand (sand wedges) (Sletten et al., 2003), (d) image of an excavation by the shovel aboard the Phoenix lander, with a subsurface perchlorate-rich zone outlined by a box labeled 2 (reproduced from Cull SC, Arvidson RE, Catalano JG, et al. (2010) Concentrated perchlorate at the Mars Phoenix landing site: Evidence for thin film liquid water on Mars. *Geophysical Research Letters* 37: L22203). With permission from John Wiley & Sons.

surface) is indicative of both alkaline pH and some modest aqueous transport. In particular, the highly soluble perchlorate appears to be largely found below the surface (**Figure 27(d)**), indicative of recent aqueous transport in a downward direction (Cull et al., 2010b).

To summarize, there is evidence of significant chemical weathering of soils in the more humid Martian past (Amundson et al., 2008), and multiple lines of evidence for relatively recent, but very modest, downward aqueous movement of water and salt at multiple locations (Amundson et al., 2008; Arvidson et al., 2010; Cull et al., 2010b). It is therefore instructive to consider the diversity of soils on Mars through the earth-based soil classification system of the USA:

- The Phoenix landing site likely has *Gelisols*, soils containing permafrost within 2 m of the soil surface and exhibiting marked evidence of cryoturbation.
- *Entisols*, soils lacking virtually any chemical alteration are certainly common.

- *Aridisols*, soils with subsurface accumulations of salts, as well as clay from chemical weathering in previous more humid conditions, appear to be present at Gusev, Meridiani Planum, and possibly other sites.

Beyond these surficial soils that are actively interacting with the atmosphere, it could be anticipated that a number of paleosols (Retallack, 2003) are embedded within the extensive sedimentary deposits on Mars. Deriving information about the climate and biota of the Martian past from these soils will involve fortuitous contact with soil exposures, and chemical analyzers on the landers that are capable of both chemical and isotopic analyses.

7.1.8 Concluding Remarks

The content of this chapter represents some of the meanders that the low temperature geochemical community has followed in the last decade. In 2004 when the previous version of this chapter was published, the geochemical interpretation of soil profiles and pore waters was in its initial phases, and we knew little at all about the soil chemistry of the hyperarid soils of either Earth or Mars.

Probably the most startling development since 2004 is how soil (and what comes from it) now matters to so many people – particularly students. It seems during the past decade that the finite nature of earth's resources, particularly soil and the products it produces or mediates, has registered with a diverse audience. "Future agricultural practices will shape, perhaps irreversibly, the surface of the Earth, including its species, biogeochemistry, and utility to society" (Tilman et al., 2002). Agriculture imparts profound changes on soil processes, including wholesale physical mixing, addition of water and reactive chemicals, erosion, and changes in biota. From both morphological and biogeochemical perspectives, these human induced changes in state factors create new soils which begin to undergo largely unknown and unstudied geochemical trajectories. A primary societal challenge – and opportunity – facing geochemists in this century is to direct efforts to soil processes occurring in the 'domesticated' landscapes of the globe and to develop an integrated understanding of how the rates of biogeochemical processes in these agricultural and urban landscapes operate.

References

Amundson R (2001) The carbon budget in soils. *Annual Review of Earth and Planetary Sciences* 29: 535–562.

Amundson R (2003) Soil Formation. In: Holland HD and Turekian KK (eds.) *Treatise of Geochemistry*, vol. 5, pp. 1–35. Oxford: Elsevier.

Amundson R, Austin AT, Schuur AG, et al. (2003a) Global patterns of the isotopic composition of soil and plant nitrogen. *Global Biogeochemical Cycles* 17: 1031. http://dx.doi.org/10.1029/2002GB001903, 2003.

Amundson R, Barnes JD, Ewing S, Heimsath A, and Chong G (2012) The stable isotope composition of halite and sulfate of hyperarid soils and its relation to aqueous transport. *Geochimica et Cosmochimica Acta* 99: 271–286.

Amundson R, Ewing S, Dietrich W, et al. (2008) On the *in situ* aqueous alteration of soils on Mars. *Geochimica et Cosmochimica Acta* 72: 3845–3864.

Amundson R, Ewing SA, and Owen JJ (2010) The Earth on the other side of life. In: *Abstract EP42A-01, Presented at 2010 Fall Meeting, 13–17 December. San Francisco, CA: AGU*.

Amundson R, Guo Y, and Gong P (2003b) Soil diversity and landuse in the United States. *Ecosystems* 6: 470–482.

Amundson R and Lund LJ (1985) Changes in the chemical and physical properties of a reclaimed saline–sodic soil in the San Joaquin Valley of California. *Soil Science* 140: 213–222.

Amundson RG and Smith VS (1988) Annual cycles of physical and biological properties in an uncultivated and irrigated soil in the San Joaquin Valley of California. *Agriculture, Ecosystems and Environment* 20: 195–208.

Arvidson RE, Bell III JF, Bellutta P, et al. (2010) Spirit Mars Rover Mission: Overview and selected results from the northern Home Plate Winter Haven to the side of Scamander crater. *Journal of Geophysical Research* 115: E00F03. http://dx.doi.org/10.1029/2010JE003633.

Arvidson RE, Ashley JW, Bell III JF, et al. (2011) Opportunity Mars Rover mission: Overview and selected results from Purgatory ripple to traverses to Endeavour crater. *Journal of Geophysical Research* 116: E00F15. http://dx.doi.org/10.1029/2010JE003746.

Banwart S, Bernasconib SM, Bloemc J, et al. (2011) Soil processes and functions in the critical zone observatories: Hypotheses and experimental design. *Vadose Zone Journal* 10: 974–989.

Beaudette DE and O'Geen AT (2009) Soil-Web: An online soil survey for California, Arizona, and Nevada. *Computers and Geosciences* 35: 2119–2128.

Beaudette DE and O'Geen AT (2010) An iPhone application for on-demand access to digital soil survey information. *Soil Science Society of America Journal* 74: 1682–1684.

Brantley SL, Bandstra J, Moore J, and White AF (2008) Modeling chemical depletion profiles in regolith. *Geoderma* 145: 494–504.

Brantley SL and Lebedeva M (2011) Learning to read the chemistry of regolith to understand the critical zone. *Annual Review of Earth and Planetary Sciences* 39: 387–416.

Brimhall G, Chadwick OA, Lewis CJ, et al. (1992) Deformational mass balance transport and invasive processes in soil evolution. *Science* 255: 695–702.

Brimhall GH and Dietrich WE (1987) Constitutive mass balance relations between chemical composition, volume, density, porosity, and strain in metasomatic hydrochemical systems: Results on weathering and pedogenesis. *Geochimica et Cosmochimica Acta* 51: 567–587.

Burt R (ed.) (2004) *Soil Survey Laboratory Methods Manual*. *Soil Survey Investigations Report No*. 42, NRCS, USDA, Washington, DC.

Burt R, Wilson MA, Mays MD, and Lee CW (2003) Major and trace elements of selected pedons in the USA. *Journal of Environmental Quality* 32: 2109–2121.

Cerling TE (1984) The stable isotopic composition of modern soil carbonate and its relationship to climate. *Earth and Planetary Science Letters* 71: 229–240.

Childers DL, Corman J, Edwards M, and Elser JJ (2011) Sustainability challenges of phosphorus and food: Solutions from closing the human phosphorus cycle. *BioScience* 61: 117–124.

Christiansen PR, Ruff SW, Fergason RL, et al. (2004) Initial results from the Mini-TES experiment in Gusev crater from the Spirit rover. *Science* 305: 837–842.

Clark BC, Baird AK, Weldon RJ, Tsusaki DM, Schnabel L, and Candelaria MP (1982) Chemical composition of Martian fines. *Journal of Geophysical Research* 87: 10,059–10,067.

Crutzen PJ (2002) Geology of mankind. *Nature* 415: 23.

Cull SC, Arvidson RE, Catalano JG, et al. (2010a) Concentrated perchlorate at the Mars Phoenix landing site: Evidence for thin film liquid water on Mars. *Geophysical Research Letters* 37: L22203. http://dx.doi.org/10.1029/2010GL045269.

Cull S, Arvidson RE, Mellon MT, Skemer P, Shaw A, and Morris RV (2010b) Compositions of subsurface ices at the Mars Phoenix landing site. *Geophysical Research Letters* 37: L24203. http://dx.doi.org/10.1029/ 2010GL045372.

Darwin C (1881) *The Formation of Vegetable Mould, Through the Action of Worms, with Observations on Their Habits*. London: John Murray.

DePaolo DJ (2004) Calcium isotopic variations produced by biological, kinetic, radiogenic and nucleosynthetic processes. *Reviews in Mineralogy and Geochemistry* 55: 255–288.

Dethier DP and Bove DJ (2011) Mineralogical and geochemical changes from alteration of granitic rocks, Boulder Creek catchment, Colorado. *Vadose Zone Journal* 10: 858–866.

Dietrich WE, Bellugi DG, Sklar LS, Stock JD, Heimsath AM, and Roering JJ (2003) Geomorphic transport laws for predicting landscape form and dynamics. *Prediction in Geomorphology*. *Geophysical Monograph* No. 135. Washington, DC: American Geophysical Union. http://dx.doi.org/10.1029/135GM09.

Ewing SA, Amundson R, Michalski G, et al. (2007) Rainfall limit of the N cycle on Earth. *Global Biogeochemical Cycles* 21: GB3009. http://dx.doi.org/10.1029/2006GB002838.

Ewing SA, Sutter B, Amundson R, et al. (2006) A threshold in soil formation at Earth's arid–hyperarid transition. *Geochimica et Cosmochimica Acta* 70: 5293–5322.

Ewing SA, Yang W, DePaolo DJ, et al. (2008) Non-biological fractionation of stable Ca isotopes in soils of the Atacama Desert, Chile. *Geochimica et Cosmochimica Acta* 72: 1096–1110.

Gellert R, Rieder R, Anderson RC, et al. (2004) Chemistry of rocks and soils in Gusev crater from the alpha particle x-ray spectrometer. *Science* 305: 829–832.

Gellert R, Rieder R, Bruckner J, et al. (2006) Alpha particle x-ray spectrometer (APXS): Results from Gusev crater and calibration report. *Journal of Geophysical Research: Planets* 111(E2): E02S05. http://dx.doi.org/10.1029/2005JE002555.

Hagedorn B, Sletten RS, and Hallet B (2007) Sublimation and ice condensation in hyperarid soils: Modeling results using field data from Victoria Valley, Antarctica. *Journal of Geophysical Research* 112: F03017.

Harden JW (1987) Soils developed in granitic alluvium near Merced, California. *U.S. Geological Survey Bulletin* 1590-A: 26.

Heimsath AM, Dietrich WE, Nishiizumi K, and Finkel RC (1997) The soil production function and landscape equilibrium. *Nature* 388: 358–361.

Jenny H (1941) *Factors of Soil Formation: A System of Quantitative Pedology*. New York: McGraw-Hill.

Johnson DL (1990) Biomantle evolution and the redistribution of earth materials and artifacts. *Soil Science* 149: 84–102.

Maher K (2010) The dependence of chemical weathering rates on fluid residence time. *Earth and Planetary Science Letters* 294: 101–110.

Maher K, Steefel CI, White AF, and Stonestrom DA (2009) The role of reaction affinity and secondary minerals in regulating chemical weathering rates at the Santa Cruz soil chronosequence, California. *Geochimica et Cosmochimica Acta* 73: 2804–2831.

McGlynn IO, Fedo CM, and McSween HY Jr. (2011) Origin of basaltic soils at Gusev crater, Mars, by aeolian modification of impact-generated sediment. *Journal of Geophysical Research* 116: E00F22. http://dx.doi.org/10.1029/2010JE003712.

McLennan SM, et al. (2005) Providence and diagenesis of the evaporate-bearing Burns formation, Meridian in Planum, Mars. *Earth and Planetary Science Letters* 240: 95–121.

Mellon MT, Malin MC, Arvidson RE, et al. (2009) The periglacial landscape at the Phoenix landing site. *Journal of Geophysical Research* 114: E00E06. http://dx.doi.org/10.1029/2009JE003418.

Merrill GP (1906) *A Treatise on Rocks, Rock-Weathering, and Soils*. New York: McMillan.

Michalski G, Bockheim JG, Kendall C, and Thiemens M (2005) Isotopic composition of Antarctic Dry Valley nitrate: Implications for NOy sources and cycling in Antarctica. *Geophysical Research Letters* 32: L13817. http://dx.doi.org/10.1029/2004GL022121.

Michalski G, Bohlke JK, and Thiemens J (2004) Long term atmospheric deposition as the source of nitrate and other salts in the Atacama Desert, Chile: New evidence from mass-independent oxygen isotopic compositions. *Geochimica et Cosmochimica Acta* 68: 4023–4038.

Monfreda C, Ramankutty N, and Foley JA (2008) Farming the planet: 2. Geographic distribution of crop areas, yields, physiological types, and net primary productivity in the year 2000. *Global Biogeochemical Cycles* 22: GB1022. http://dx.doi.org/10.1029/2007GB002947.

Montgomery DR (2007) Soil erosion and agricultural sustainability. *Proceedings of the National Academy of Sciences of the United States of America* 104: 13268–13272.

Owen JJ, Amundson R, Dietrich WE, Nishiizumi K, Sutter B, and Chong G (2011) The sensitivity of hillslope bedrock erosion to precipitation. *Earth Surface Processes and Landforms* 36: 117–135.

Pavich MJ, Brown L, Harden J, Klein J, and Middon R (1986) ^{10}Be distribution in soils from Merced River terraces, California. *Geochimica et Cosmochimica Acta* 50: 1727–1735.

Post WM, Emanuel WR, Zinke PJ, and Stangenberger AG (1982) Soil carbon pools and world life zones. *Nature* 298: 156–159.

Quade J, Cerling TE, and Bowman JR (1989) Systematic variations in the carbon and oxygen isotopic composition of pedogenic carbonate along elevation transects in the southern Great Basin, United States. *Geological Society of America Bulletin* 101: 464–475.

Quinton JN, Govers G, Van Oost K, and Bardgett RD (2010) The impact of agricultural erosion on biogeochemical cycling. *Nature Geoscience* 3: 311–314.

Railsback BL (2003) An earth scientist's periodic table of the elements and their ions. *Geology* 31: 737–740.

Rasmussen C, Brantley S, Richter D deB, Blum A, Dixon J, and White AF (2011) Strong climate and tectonic control on plagioclase weathering in granitic terrain. *Earth and Planetary Science Letters* 301: 521–530.

Raymond PA and Cole JJ (2003) Increase in the export of alkalinity from North America's largest river. *Science* 301: 88–91.

Rech JA, Quade J, and Hart WS (2003) Isotopic evidence for the source of Ca and S in soil gypsum, anhydrite and calcite in the Atacama Desert, Chile. *Geochimica et Cosmochimica Acta* 67: 575–586.

Reed S and Amundson R (2007) Sediments, gophers, and time: A model for the origin and persistence of Mima mound-vernal pool topography in the Great Central Valley. In: Schlising RA and Alexander DG (eds.) *Vernal Pool Landscapes*, pp. 15–27. Chico: California State University.

Reed S and Amundson R (2012) Using LIDAR to model Mima mound evolution and regional energy balances in the Great Central Valley, California. In: *Horwath Burnham JL and Johnson DL* (eds.) *Mima Mounds: The Case for Polygenesis and Bioturbation*, pp. 21–41. Geological Society of America Special Paper 490, http://dx.doi.org/10.1130/2012.2490(01).

Retallack GJ (2003) Soils and global change in the carbon cycle over geological time. In: Holland HD and Turekian KK (eds.) *Treatise on Geochmistry*, vol. 5, pp. 581–605. Oxford: Elsevier.

Riebe CS, Kirchner JW, and Finkel RC (2004) Erosional and climatic effects on long-term chemical weathering rates in granitic landscapes spanning diverse climate regimes. *Earth and Planetary Science Letters* 224: 547–562.

Riebe CS, Kirchner JW, Granger DE, and Finkel RC (2001) Strong tectonic and weak climatic control of long-term chemical weathering rates. *Geology* 29: 511–514.

Sanchez PA, Ahamed S, Carré F, et al. (2009) Digital soil map of the world. *Science* 325: 680–681.

Scanlon BR, Jolly I, Sophocleous M, and Zhang L (2007) Global impacts of conversions from natural to agricultural ecosystems on water resources: Quantity versus quality. *Water Resources Research* 43: W03437. http://dx.doi.org/10.1029/2006WR005486.

Schertz DL (1983) The basis for soil loss tolerances. *Journal of Soil and Water Conservation* 38: 10–14.

Sletten RS, Hallet B, and Fletcher RC (2003) Resurfacing time of terrestrial surfaces by the formation and maturation of polygonal patterned ground. *Journal of Geophysical Research* 108(E4): 8044. http://dx.doi.org/10.1029/2002JE001914, 2003.

Smil V (2004) *Enriching the Earth*. Cambridge, MA: MIT Press.

Stallard RF (1998) Terrestrial sedimentation and the carbon cycle: Coupling weathering and erosion to the carbon cycle. *Global Biogeochemical Cycles* 12: 231–257.

Steefel CI and Lasaga AC (1994) A coupled model for transport of multiple chemical-species and kinetic precipitation dissolution reactions with application to reactive flow in single-phase hydrothermal systems. *American Journal of Science* 294: 529–592.

Stonestrom DA, Scanlon BR, and Zhang L (2009) Introduction to special section on impacts of land use change on water resources. *Water Resources Research* 45: W00A00. http://dx.doi.org/10.1029/2009WR007937.

Tilman D, Cassman KG, Matson PA, Naylor R, and Polasky S (2002) Agricultural sustainability and intensive production practices. *Nature* 418: 671–677.

Trumbore SE, Chadwick OA, and Amundson R (1996) Rapid exchange between soil carbon and atmospheric carbon dioxide driven by temperature change. *Science* 272: 393–396.

Ugolini FC and Anderson DW (1973) Ionic migration and weathering in frozen Antarctic soils. *Soil Science* 115: 461–470.

van Oost K, Quine TA, Govers G, et al. (2007) The impact of agricultural soil erosion on the global carbon cycle. *Science* 318: 626–629.

Walvoord (2002) *A Unifying Conceptual Model of Water, Vapor and Solute Movement in Deep Arid Vadose Zones*. PhD Dissertation, New Mexico Tech, Socorro, NM.

Wang Y, McDonald E, Amundson R, McFadden L, and Chadwick O (1996) An isotopic study of soils in chronological sequences of alluvial deposits, Providence Mountains, California. *Geological Society of America Bulletin* 108: 379–391.

Wang A, Haskin LA, Squyres SW, et al. (2006) Sulfate deposition in subsurface regolith in Gusev crater, Mars. *Journal of Geophysical Research* 111: E02S17. http://dx.doi.org/10.1029/2005JE002513.

White AF (2002) Determining mineral weathering rates based on solid and solute weathering gradients and velocities: Application to biotite weathering in saprolites. *Chemical Geology* 190: 69–89.

White AF, Blum AE, Schulz MS, Bullen TD, Harden JW, and Peterson ML (1996) Chemical weathering rates of a soil chronosequence on granitic alluvium. 1. Quantification of mineralogical and surface area changes and calculation of primary silicate reaction rates. *Geochimica et Cosmochimica Acta* 60(14): 2533–2550.

White AF, Schulz MS, Vivit DV, Blum AE, Stonestrom DA, and Anderson SP (2008) Chemical weathering of a marine terrace chronosequence, Santa Cruz, California I: Interpreting rates and controls based on soil concentration-depth profiles. *Geochimica et Cosmochimica Acta* 72: 36–68.

White AF, Schulz MS, Stonestrom DA, et al. (2009) Chemical weathering of a marine terrace chronosequence, Santa Cruz, California II: Controls on solute fluxes and comparisons of long-term and contemporary mineral weathering rates. *Geochimica et Cosmochimica Acta* 73: 2769–2803.

Williams JZ, Bandstra JZ, Pollard D, and Brantley SL (2010) The temperature dependence of feldspar dissolution determined using a coupled weathering-climate model for Holocene-aged loess soils. *Geoderma* 156: 11–19.

Yoo K, Amundson R, Heimsath AM, Dietrich WE, and Brimhall GH (2007) Integration of geochemical mass balance with sediment transport to calculate rates of soil chemical weathering and transport on hillslopes. *Journal of Geophysical Research* 112: F02013. http://dx.doi.org/10.1029/2005JF000402.